Science and Global Security, 18:1–60, 2010

ISSN: 0892-9882 print / 1547-7800 online
DOI: 10.1080/08929880903422034

Routledge
Taylor & Francis Group

Assessment of Long Range Laser Weapon Engagements: The Case of the Airborne Laser

Jan Stupl[1] and Götz Neuneck[2]

[1]Center for International Security and Cooperation (CISAC), Stanford University, Stanford, California, USA
[2]Institute for Peace Research and Security Policy (IFSH) at the University of Hamburg, Hamburg, Germany

This article presents a method developed to assess laser Directed Energy Weapon engagements. This method applies physics-based models, which have been validated by experiments. It is used to assess the capabilities of the Airborne Laser (ABL), a system for boost phase missile defense purposes, which is in development under supervision of the U.S. missile defense agency. Implications for international security are presented.

The article begins with a general introduction to laser Directed Energy Weapons (DEW). It is notable that several laser directed energy weapon prototypes have recently become operational for testing. One of them is the ABL, a megawatt-class laser installed into a cargo aircraft. It is concluded that only the ABL could have significant political impact on an international scale at the moment. Hence, the remainder of the article focuses on the assessment of that system. The laser intensity, the induced temperature increase of a target and the impact of this temperature increase on the mechanical properties of the target are calculated for different scenarios. It is shown that the defensive capability of the ABL against ballistic missiles is limited. Even a successful laser engagement that deflects a missile trajectory from its intended target can have negative impact for third parties, as missile warheads will most likely not be destroyed.

INTRODUCTION

The first laser was put into operation by Theodore Maiman in 1960.[1] Today, lasers are widely employed in civilian and military settings. Civilian applications include CD-players and laser welding, using power levels between milliwatts and kilowatts. In the military arena, laser ranger finders and laser guided bombs have been used since the 1970s.[2] In the case of range finders and

Received 12 July 2009; accepted 12 November 2009.
Address correspondence to Jan Stupl, Center for International Security and Cooperation (CISAC), Stanford University, Encina Hall, 616 Serra Street, Stanford, CA 94305-6165. E-mail: stupl@stanford.edu

laser guidance, the laser energy is not directly responsible for target damage, the laser is only used as part of another weapon's targeting system. The term *laser weapon* implies the use of lasers as *directed energy weapons (DEW)*. In that case, the laser energy is causing the target damage. Some trace the idea of such weapons back to the alleged use of focused sunlight by the Greek philosopher Archimedes during the battle of Syracuse. However, so far the use of lasers in battle has been limited to one application only, namely laser blinding weapons. This happened during the Falklands[3] conflict and the 1980s war between Iran and Iraq,[4] before the protocol on laser blinding weapons was established in 1995.[5] After 1995, only some single incidents are quoted in newspaper articles, e.g., U. S. helicopter pilots allegedly have been targeted by a Russian merchant ship near the U. S. coast in 1997, by Serbian troops over Bosnia in 1998, and by North Korean forces near the demilitarized zone in 2003.[6]

The use of laser DEW against military hardware has not taken place in the battlefield, yet. This is despite huge funding efforts by the U. S. government since the 1960s, which led to the development of lasers with continuous output powers in the kilowatt range shortly after Maiman's discovery. Already in 1968 Gerry accomplished a continuous power level of 138 kW using a gasdynamic CO_2 laser,[7] and in 1980 two megawatts were reached by the Mid-infrared advanced chemical laser (MIRACL).[8] However, these technological accomplishments did not lead to the deployment of weapon systems. One reason for that is the challenge is not only to build a laser with a high output power but also to integrate it into a functional weapon system. This weapon system would have to include the laser source, the necessary optics to focus the beam at the desired distance, means for target detection and target tracking, and measures to track the target with the laser beam, e.g., a fast steering mirror. Finally, a real-time computer system is needed to control the different components.

From a military point of view, all these components have to be combined into a system that is deployable in a military setting and offers advantages over existing weapon systems, in order to warrant the development costs and acquisition. From a policy standpoint, it is also desirable that those new abilities are not destabilizing to international relations, as described later. At the moment, several laser DEW systems are in development. The most prominent example for a contemporary laser DEW is the *Airborne Laser* (ABL) missile defense program.

The goal of the ABL is the destruction of ballistic missiles in their boost-phase. The boost-phase is the time during the ascent of a missile when the engine is active and accelerating the missile. This implies a highly visible target, as the engine is sending out hot gases, which are easily detectable by infrared sensors. After the end of the boost-phase, the missile will follow a ballistic trajectory, which ends with the re-entry of the warhead into the atmosphere and the impact onto the target. For that reason, the time-line of an ABL

engagement is crucial.[9] If the ABL is not able to inflict significant damage to the missile before the end of the boost phase, the missile will reach its final velocity and therefore its target, even if the missile is damaged later. If laser damage causes a shortened boost phase, the timing of the ABL engagement will determine the final velocity and therefore the missile's point of impact. At any point of impact, severe damage is possible, as the ABL will not be able to destroy a warhead for most scenarios.

If the ABL program is successful, it would give the United States its first ability for boost phase missile defense. This task is not achievable by other means at the moment. Therefore, there are also strong political implications. In order to assess the political implications of any laser DEW system, is it necessary to understand its technical abilities and shortcomings.

After a general introduction to the background and recent developments in the field of laser DEW, the second part of this article will describe a method developed to assess the effects on a target engaged by laser DEW, focusing on missile defense applications. This method was validated using scaled experiments. As an example, a scenario is assessed which involves an ABL engagement against a midrange liquid fuel missile flying from North Korea to Japan. This and further scenarios, summarized in the third part of this article are used to provide an independent assessment of the ABL's capabilities. In general this article follows a best case approach, in order to assess whether long range laser weapons could have any usability today. This research builds upon the research undertaken by the American Physical Society Study Group on Boost-Phase Intercept Systems.[10] This article extends their work especially in the field of interaction between laser and target.

INTRODUCTION TO LASER DIRECTED ENERGY WEAPONS

Technical Implications

Laser DEW propagate energy between the weapon and the target by the means of a laser beam. A successful engagement implies that the target is heated up to a point where it ceases to operate effectively. From a military point of view, there are several advantages and disadvantages to using laser DEW compared to projectile weapons. The potential advantages of laser DEW are several:

- Laser beams propagate at the speed of light. This vastly simplifies targeting, as there is no need to calculate the trajectories of projectiles. The laser beam will travel approximately in a straight line for several hundred kilometers. In addition, this complicates evasive maneuvers for a potential target.

- Tracking the target with the beam is accomplished by moving a mirror. As mirrors are less massive than gun turrets, they can be moved faster, enabling tracking of highly maneuverable targets.
- Laser DEW do not use ammunition in the sense of a magazine of projectiles. Instead, the laser has to be powered. The power source depends on the type of the laser, and will be electric for many cases, not including the Airborne Laser. As long as there are means to power the laser and the laser itself can sustain continuous operation, there are no limits in the laser's time of operation. In practice this scenario might work for an electric laser onboard an aircraft carrier, where there is a nearly unlimited power source. Laser weapons for an infantry soldier will likely stay in the realm of science fiction for some time, due to lack of a transportable power supply.
- Effects on a target can be adjusted if a laser with variable output power is used. Prerequisite for that are that both the resulting laser intensity on target as well as the damage mechanism are well understood. For example, whether a soldier is just dazzled or blinded by a laser weapon depends on many factors, including the ambient light, the weather and whether the soldier wears eyeglasses.

Depending on the scenario, these advantages have to compete with a range of unique disadvantages, including:

- There has to be a line of sight between the laser and the target. This requirement might be negated by relay mirrors, but those complicate the tracking process.
- Atmospheric effects can negatively affect laser beam propagation. Absorption, scattering and turbulence have to be taken into account, if the beam travels in the atmosphere. Depending on the range and the atmospheric conditions, it might not be possible to employ a laser at all. Especially adverse conditions include rain, fog, or smoke.
- As soon as critical laser intensities are reached, non-linear effects set in. The laser itself influences the atmosphere, starting with simple heating effects and culminating in ionization if the laser intensity reaches sufficient levels. Somewhere between those extremes, the absorption coefficient becomes a function of laser intensity. For that reason, the maximum intensity which can be transported through a given path is limited. Non-linear effects especially become important if short-pulsed lasers with high intensities are used. Critical intensities depend on the wavelength. For lasers with a wavelength of 1.3 μm this intensity is in the order of megawatts per square centimeter.[11] Please note that for the cases examined in this study, non-linear absorption is not relevant, as intensities are not reaching those levels.

- In contrast to conventional ammunitions, which release their kinetic and/or chemical energy with no noticeable time delay upon impact, a laser usually needs some time to heat up the exposed target area until significant damage occurs. The tracking mechanism of the laser system has to be able to track the target during that time.
- In addition to conventional defensive measures, laser radiation can be deflected by highly reflective coatings. For a given wavelength, a reflectivity of up to 99 percent can be accomplished by simple thin coatings. Multi-layer coatings can further increase the reflectivity. Further counter measures include a fast target movement in order to spread the laser energy or ablative coatings.
- In the past, lasers have often been big, fragile optical instruments. Laser optics have to be protected against contaminants as well as misalignments.

The last point alone has probably played a decisive role in preventing the deployment of laser weapons until now. However, recent developments might change that picture.

Recent Developments in Laser DEW

Contemporary development of laser DEW systems can be put into two categories, *industry funded projects that use civilian off-the-shelf industrial lasers* and *government funded research, which aims at high power laser systems*. The latter research aims at continuous power levels exceeding civilian lasers by one or two orders of magnitude. Laser sources developed for those projects have no industrial applications at the moment. Major defense companies in the United States and elsewhere[12] are working on both tracks.

Laser DEW Prototypes Using Civilian Laser Technology

Boeing and Raytheon recently introduced tactical laser weapon demonstrators using industrial solid-state lasers. Boeing modified an "Avenger" air defense vehicle mounting ground to air missiles. They replaced one of the missile launchers with a laser DEW. As a laser source, this system uses a commercial 2 kW solid state laser. The new "Laser Avenger" has been used to track and destroy an unmanned aerial vehicle as well as explosive devices on the ground.[13] In a press release Boeing points out that this system would not reveal its position by missile exhaust or gun flashes, citing that as an advantage in comparison to conventional systems.[14] While this is a valid point at the moment, the scattered light[15] of the Avenger's 2 kW infrared laser beam could also be used by opponents to detect the vehicle in the future.

Boeing is also working on a higher power weapon demonstrator. The Relocatable High Energy Laser System (RHELS) is combining four industrial

thin-disk lasers into a 10 kW system. Those lasers are usually used in the manufacturing industry, e.g., for welding in automotive applications.[16] The RHELS consists of the lasers as well as components for cooling, power supply and tracking. All components are installed in a 40-foot shipping container. This relocatable approach has been chosen in order to test this demonstrator in different locations.

Industrial fiber lasers manufactured by the company IPG Photonics are used by Raytheon in its Laser Area Defense system (LADS). The LADS is a weapon demonstrator which is based on a modified Phalanx air-defense system. The conventional Phalanx system uses radar controlled multi-barreled cannons. Phalanx is installed on some U.S. Navy ships in order to protect them against close in missile targets. Raytheon has replaced the cannons with a laser. The modified system is being tested against a variety of targets, including incoming mortar rounds.[17]

The thin-disk lasers and fiber lasers, which are employed in the last mentioned systems, are two approaches used in the manufacturing industry to scale solid-state lasers to higher power levels. The major challenge on that method is the limited efficiency of the energy conversion processes which create the laser beam. Because of that, a major part of the energy used to create the beam is lost as excess heat. This excess heat occurs inside the light amplifying medium of the laser, which creates the beam. For a solid-state laser, this is a crystal. The produced excess heat has to be transported out of the solid-state medium, in order to avoid overheating and, finally, destroying the laser. In addition, a non-uniform temperature distribution inside the amplifier causes a higher than ideal beam divergence of the resulting laser beam. This means that the beam spreads out further with traveled distance than in the ideal case and less energy per target area is delivered. To avoid that, the light amplifying medium has to be cooled in a way which results in a regular temperature profile. Increasing the surface of the amplifier simplifies cooling. Hence, the geometry of the active medium is optimized. In the past voluminous rods have been used, now thin disks or optical fibers are used as laser amplifiers. The result is a better beam quality, hence a lower divergence at high power levels compared to a standard rod configuration. In addition to the increased surface, fiber lasers have the further advantage that the ends of the fiber itself are used to form the laser resonator. This allows a ruggedized design, as no mirror alignment is necessary. That is especially important for military laser applications. Fiber lasers are a recent development which introduced changes into the market for industrial lasers and might also lead to further development in military lasers. At the moment, fiber lasers deliver the highest continuous output powers of all commercial lasers. The company IPG offers fiber lasers with a power up to 50 kW. Nevertheless, the need to cool fiber and disk solid-state lasers puts a limit to their maximum power.

Military Laser DEW Developments

U.S. government funded programs on solid-state lasers have so far reached power levels in the same order of magnitude as the lasers described above. Recently, Northrop Grumman has announced the successful test of a 100 kW solid-state laser, as part of the Joint High Power Solid State Laser program.[18] This is generally seen as a power level at which lasers become useful for tactical applications. For strategic applications, laser power in the megawatt range is desirable. Such power levels can be achieved by chemical lasers, which have been developed for military programs.[19] In contrast to electrical powered solid-state and semiconductor lasers, chemical lasers use a chemical reaction to create the beam. The involved chemical agents are fed continuously into the reaction chamber. These agents form a gas stream, which is the light amplifying medium for this class of lasers, as depicted in Figure 1. The gas stream is continuously produced and the old reactants are vented out of the laser. Therefore, excess heat does not accumulate and the output power is not limited by the need for cooling.

At the moment there are two U. S. laser DEW systems which are employing chemical lasers. Those are the Advanced Tactical Laser (ATL) and the Airborne Laser (ABL). Both systems use airplanes as platforms for the laser DEW. The ATL is a technology demonstrator built to evaluate the abilities of a laser DEW for "ultra-precision" attacks, e.g., against communication platforms or vehicles.[20] The range is in the order of 10 to 20 km.[21] The ATL is using a Chemical Oxygen Iodine Laser (COIL) with undisclosed output power. Different sources quote values between several tens of kilowatts and 300 kW.[22] Basis for the ATL is a standard C-130 cargo aircraft. As possible engagements, covert operations are mentioned, as well as settings where civilian assets are mixed with military targets.[23] The ATL project started in 2002 using funding by the U.S.

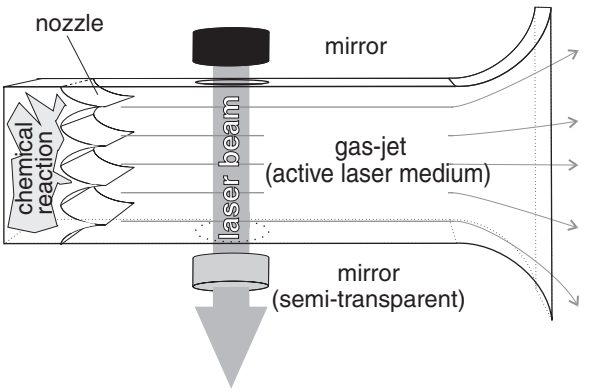

Figure 1: Working principle of a chemical laser. The laser energy is provided by a chemical reaction, which produces a continuous gas jet. The gas jet is the active (light amplifying) laser medium.

Special Operations Command. Late in 2008, the prototype was tested against a ground target. Further testing has been funded by the U.S. Air Force.[24] A first in-flight test occurred in June 2009.[25]

The Airborne Laser (ABL) is the most prominent contemporary laser DEW program. It is built around a basic Boeing 747 aircraft, which is outfitted with a COIL with a continuous output power in the megawatt range (the exact value is classified). Its primary goal is boost-phase missile defense over strategic ranges of several hundred kilometers.[26] In order to achieve this mission, one ABL is to be on station, near possible missile launch sites all the time. At the moment of a missile launch, the ABL would then attack the missile. In addition to the main laser, sensor and tracking equipment, the ABL also features an adaptive optic component, which is supposed to correct the degrading influence of atmospheric turbulence on the laser beam. This component is crucial to reach the intended range. This article uses ABL engagement scenarios for a case study. Further technical details about the ABL's setup are provided in the Appendix to this paper. Additional details can also be found in the literature.[27]

The ABL program was initiated in 1994.[28] Until 2008, approximately $5 billion have been spent on the system.[29] Originally, a first test of the system against a test missile was scheduled for 2002.[30] This test has been postponed several times, recently to late 2009 or early 2010.[31] Nevertheless, some progress has been made. In 2008, all the components were finally installed inside the aircraft and the high energy laser was activated for the first time on the ground.[32] Flight worthiness was certified in April 2009.[33] At the moment, further tests of the components are underway, culminating in the scheduled flight tests against boosting SCUD-type missiles. The current administration has shifted the program from procurement to a pure research and development program and delayed the planned purchase of a second plane, as doubts remain as to whether the system will have any operational capability.[34] After the scheduled tests it will be decided whether the program will continue or will be canceled.[35]

Implications for International Security

Depending on their abilities, laser DEW may or may not have a significant impact on international security. An impact can be expected if a system introduces new capabilities which cannot be achieved by other means. These systems could then be categorized as revolutionary systems. If a laser DEW just replaces existing conventional systems, without extending their capabilities, there will be no significant impact, just an evolution of current technical systems. For example, clandestine and ultra-precision strikes are already possible today, using guided ammunition or special forces on the ground. Hence the Advanced Tactical Laser's impact on international politics will be only minor, even if its technology might be revolutionary. On the contrary, the ABL's impact

could be huge, as the ABL could be the first operational U. S. boost-phase missile defense system. In that role, it could be used by the United States against small states, but it also might interfere with the nuclear deterrent capacity of major nuclear weapon states by attacking ICBMs in a retaliatory strike.

In addition to missile defense, the U.S. Air Force has also considered other applications for the ABL, including anti-satellite engagements.[36] Those capabilities are not mentioned by the Missile Defense Agency, which is overseeing the ABL program at the moment. Anti-satellite (ASAT) laser engagements would be a revolutionary application, as they would in principle enable an option of attacks on satellites with only minor debris. At the moment, attacking satellites implies the use of missiles with kinetic or explosive warheads. A kinetic impact creates debris, which would be harmful to the attacker's space assets, too. For that reason, space-faring nations are discouraged from using kinetic energy attacks. This fact enacts a kind of "natural" arms control. Lasers could change this situation if they are used to heat up satellites just to a point where their electronics are damaged or only to impair their sensors. Hence, attacks on satellites would be more likely, if laser DEW with anti-satellite capabilities are fielded in peacetime. In a time of crisis, this would create additional political instabilities, as satellites are important early warning and reconnaissance assets.

In order to evaluate the political implications of a specific laser weapon, it is necessary to assess its technical capabilities. To achieve this goal, a method has been devised to assess laser DEW engagements. The next section of this article describes its application for the assessment of a missile defense scenario involving the ABL. The ABL has been chosen because it is today the most advanced laser DEW with implications for international security, be it for missile defense or as laser ASAT.

ASSESSMENT OF ABL MISSILE DEFENSE ENGAGEMENTS

Outline of Assessment Method and Case Study

The flowchart presented in Figure 2 illustrates the assessment method which was used to model the impact on an irradiated target. It was developed as part of one of the author's PhD thesis.[37] Please refer to the acknowledgements of this paper for a list of involved institutions.

Laser DEW induce a heat flux on a target. Hence, the first step of the assessment method is to calculate the achievable laser intensity at the target position. This incoming intensity is partially absorbed by the target, resulting in a temperature increase over time, which is calculated during the second step of the assessment. The third step is damage assessment. In the case where the temperature rises above the melting point, significant damage of the irradiated target is unavoidable. If the melting point is not reached, a more nuanced

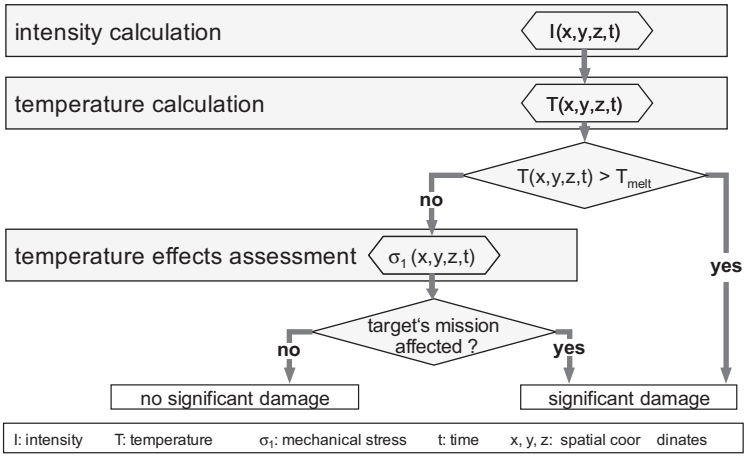

Figure 2: Flowchart of the assessment of a laser DEW engagement. The laser intensity, as well as effects on a target are evaluated in order to find out whether significant damage is inflicted by the laser weapon.

damage assessment is necessary. For example, an elevated temperature can negatively impact the tensile strength of metals and a structural element might fail before melting occurs. To assess the temperature effects in this case, it is necessary to compare the occurring mechanical stresses with the temperature dependent tensile strength of the material.

Parts A to C of the appendix describe the outlined steps in further detail. The presented theoretical background is applied to a missile defense case study, in which detailed results are intertwined after each section of the appendix. At this point, only a short summary is given.

The case study assesses a scenario for an ABL engagement against a medium range liquid fuel ballistic missile heading from North Korea to Japan. A liquid fuel missile has been chosen, because an attack against such a missile is more likely to succeed than an attack against solid propellant missiles.[38] Whether a missile can be intercepted successfully depends on the technical parameters of the missile and the ABL as well as the geometric setup, i.e., the changing distance between the missile and the ABL. The missile's technical parameters can be found in Appendix D and are inspired by the analysis of the Nodong missile by Wright and Kadyshev.[39] The technical parameters to assess the ABL performance are introduced during the course of detailed assessment presented in Appendix A. The initial positions of the ABL and the missile in the scenario are setup as illustrated in Figure 3. They have been chosen in order to accommodate two assumptions:

1. The ABL has to stay out of range of surface to air missiles.
2. Missiles will be started from a position as far as possible from the coast.

Figure 3: Setup of the missile defense scenario, which is used as an illustrative example in this article.

The first assumption arises, because the ABL is itself a highly visible target and not very maneuverable, as its platform is a Boeing 747 aircraft. There are reports that North Korea is in possession of air defense missiles with a range of 200 km.[40] Hence, the distance between the ABL and North Korea's coast has been chosen to put the ABL in a safe position. The second assumption flows from the likelihood that a country that wants to launch a missile will seek to maximize the chance of a successful missile flight in the presence of an ABL. For this medium range scenario, the easiest way to do so is to increase the distance between the missile and the ABL. For short range missiles other measures might apply.

The trajectory of the missile following this initial position is calculated using the program GUI_Missile_Flyout by Geoffrey Forden.[41] Using the result and the position of the ABL, the time-dependent intensity on the target can be derived. Appendices A, B, and C then show the details of the calculations necessary to assess the effectiveness of the missile defense engagement. Appendix A analyzes the intensity on target that might be achieved. Appendix B takes this result to calculate the elevation in target temperature that could be effected. The temperature rise thus calculated is unlikely to cause melting of the target. However, in principle, the combination of temperature induced loss in tensile strength, thermal expansion and applied mechanical stress during the missile's boost phase could lead to the missile's failure to reach the intended target, a phenomenon analyzed in Appendix C. Please refer to Tables 2, 3 and 4 in Appendix A,B and C for a summary of the input parameters.

The intensity on target will depend upon the laser beam diameter for vacuum beam propagation, on the intensity reduction due to atmospheric absorption and scattering, and the effectiveness of adaptive optics to compensate for atmospheric turbulence. Figures 14 to 16 in Appendix A show the results of

the intensity calculations under different assumptions, especially on the effectiveness of the adaptive optics performance. As explained in Appendix A, the adaptive optics' correction is initiated by a so-called beacon laser, used to measure and to allow compensation for the effects of turbulence. It will be most effective when the angle between the paths of the beacon and the weapon laser is as small as possible. The term "anisoplanatism" refers to the diversion of the two paths, and in the calculation two cases are examined—full anisoplanatism where the diversion is growing rapidly over time, attenuating the intensity of the weapon laser, and reduced anisoplanatism, which gives the best results for the weapon laser. Please refer to Appendix A for details about the technology involved.

Given the range of those assumptions, the maximum intensity at target would be about 300 watts per square centimeter, an intensity which could be reached only near the end of the boost phase of the missile under attack, and it could be much less. (This assumes that the power of the weapon laser is 3 MW. Please refer to Appendix A for an explanation, why this number is chosen). During the first 20 seconds or so of the missile launch, while the missile is still in the lower atmosphere, the laser transmittance would be too low to be effective.

The rise in target temperature will depend, of course, initially on the delivered intensity; but it will also depend significantly on the wall material of the missile being attacked, the wall thickness, the surface absorption, the initial temperature at the wall, the environment of the wall (e.g., liquid fuel) and the time on target of the laser. The detailed calculations shown in Appendix B indicate that given the range of assumptions considered, the maximum temperature on the missile that could be inflicted during its boost phase would not exceed the melting temperature of aluminum. The temperature rises imposed could, however, lower the tensile strength of the wall material, enabling the mechanical stresses to cause missile failure, the subject of Appendix C. In this Appendix, we calculate, under different assumptions on the effectiveness of adaptive optics, the earliest flight times where the stress exceeds the elastic limits of the missile shell. At this point, extensive deformations are, in principle, possible, enabling failure modes described in the next section. For reasons explained, the warhead and engine of the missile are unsuitable targets.

Impact on Warhead Trajectories

The calculations presented in the appendices indicate flight times of 47 s and 68 s as the earliest flight times for the presented case, where the stress exceeds the elastic limit. The missile model employs a boost phase of 70 s. The calculated times are valid for intensity distributions according to reduced anisoplanatism and full anisoplanatism, while the effects of liquid cooling by the fuel on the inside and aerodynamic heating by the supersonic airflow on the outside of the tank section are neglected.

The missile can fail in two different modes.[42] With rising temperatures, material strength diminishes. This either could lead to (localized or extensive) rupture of the missile wall or to a collapse of the entire structure, if large enough portions of the wall are weakened and are no longer able to bear the applied mechanical loads. This collapse could start before ruptures appear. However, as long as the stress is below the elastic limit, by definition (see Appendix C), only minimal deformation occurs, and neither of the described failure modes will take place.

After the elastic limit is exceeded, failure is in principle possible. Which mode occurs, depends on numerous factors, among others the fracture mechanics of the material of the specific missile. Depending on the failure mode, various effects can influence the warhead trajectory.

Fuel venting through a small hole in the tank might shield and/or cool the surrounding area and deny further laser impact at this position. However, the venting fuel is lost for acceleration and the trajectory will be shortened. The maximum effect for this case would be an instantaneous cut-off of the thrust. In that case, the warhead would continue on a trajectory determined by the forward momentum it already gained until this point. This would also be the case, if the warhead separates from the booster after a destructive event, e.g., the collapse of the booster. If the booster collapses and the warhead stays attached to the deformed debris, this would have an impact on the aerodynamics of the warhead. The effects vary, depending on ambient pressure, and hence the altitude when this happens. Finally, the booster could also keep accelerating the missile, but in a different direction. A change in course could be induced by a missile deformation or venting fuel. In general, the fuel remaining at the time the elastic limit is reached could accelerate the missile in an arbitrary direction.

In order to quantify the different effects and to narrow down possible impact points, the missile trajectory calculations are repeated, using the same parameters for missile thrust and masses, but cutting off the thrust at 47 s and 68 s. In the first case, the missile would only fly approximately 200 km and the trajectory would end in North Korea. If the missile is accelerating for 68 s, the changed trajectory still ends in the vicinity of its original target. The calculations are also repeated with changed aerodynamics. For the first case (cutting of the thrust and increasing the aerodynamic drag at 47 s to an (unlikely) maximum), the increased drag reduces the range another 25 percent.[43] For the second case, the effects of the increased drag are negligible at 68 s, as the missile already has reached an altitude of more then 35 km.

Please note that so far the effects of liquid cooling and aerodynamic heating have been neglected. If the effect of liquid cooling is still neglected, but aerodynamic heating is taken into account, the initial wall temperature T_0 at the beginning of the laser engagement is higher than 293 K, which was assumed for the presented results. Table 1 shows the effect of different initial

Table 1: Minimum flight time $t_{R_{p0.2}}$ until the elastic limit is reached. The result of a variation in initial temperature is shown for the case of full anisoplanatism. For $T_0 = 433$ K the aim point (represented by t_{opt}) was changed in order to minimize $t_{R_{p0.2}}$.

T_0/K	293	363	433
t_{opt}/s	60	60	55
$t_{R_{p0.2}}$/s	68	64	58

temperatures T_0 on the missile flight time $t_{R_{p0.2}}$ which is passed until the elastic limit (represented by the stress $R_{p0.2}$) is reached. The time t_{opt} represents the chosen aim point, as described in Appendix A. For T_0 a maximum of 433 K is chosen, because that is the temperature on the tip of the Ariane-1 missile at the end of its boost-phase.[44] A temperature of this magnitude is not to be expected at the missile wall, however, it can be seen as an unrealistically high upper boundary to assess the maximum effect.

To illustrate the effect of the different results on the warhead's trajectory, the impact points for the case of an instantaneous engine failure at $t_{R_{p0.2}}$ are marked in Figure 4. In addition, the original trajectory and a trajectory for an engine cut-off at 64 s are indicated. Also indicated is the area, which can be reached if the engine does not cease to function and the remaining fuel for $t_{R_{p0.2}} = 64$ s and 58 s is used for accelerations in arbitrary directions. For the case of full anisoplanatism, all impact points are far away from the location of the missile launch. Please note that the warhead will likely be intact and even if the intended target is not reached, an explosion can still cause great damage.

Countermeasures

So far the case of a conventional liquid fuel missile was modeled according to available information on the Nodong missile. In case the ABL becomes operational in the future, missile forces around the world will start to look into countermeasures against laser missile defense. Countermeasures can be developed with different levels of complexity. The simplest approach for a missile made of aluminium would be to strip down the paint and polish the surface. The difference in absorption, which could be diminished from 0.10 to 0.04 would be enough to prevent a significant temperature increase for the presented case study, see Figure 5 b).[45] As an aluminium surface tends to oxidize quickly, this might not be practical without additional measures. Measurements by Freeman et al. show an increase in absorption at the ABL's wavelength to 0.11, if a polished sample is weathered for three months.[46] To prevent this, anti-corrosive paint is not an option, as its absorption will most likely be higher than the absorption of a polished surface, hence negating the

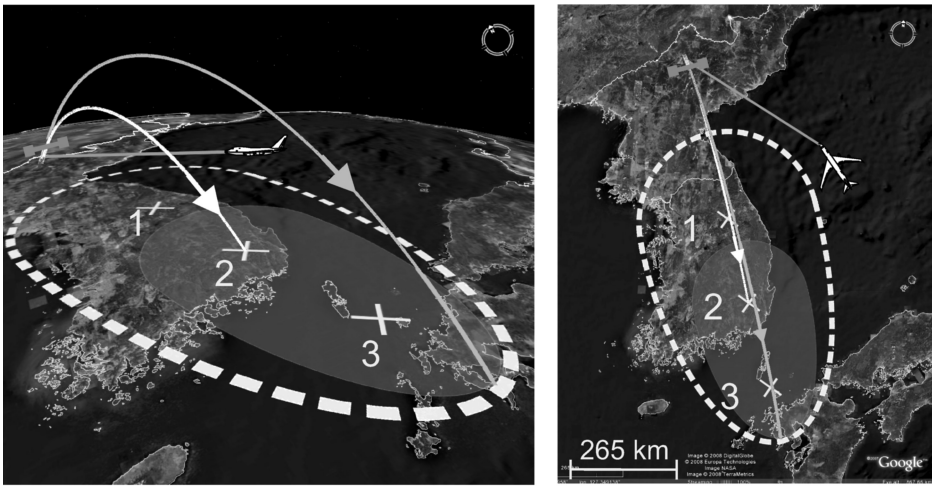

laser beam at $t_F = t_{opt}$

end of boost phase (70 s)

original trajectory (70 s boost phase)

trajectory resulting of a 64 s boost phase
(engine cut-off at $t_F = t_{Rp0.2}$= 64 s)

reachable area with remaining fuel at $t_F = t_{Rp0.2}$ = 58 s

reachable area with remaining fuel at $t_F = t_{Rp0.2}$ = 64 s

1, 2, 3 impact points for engine cut-off at t_F = 58 s , 64 s, 68 s

Figure 4: Possible warhead impact after an ABL engagement. Evaluated are possible scenarios after the elastic limit is reached at the flight time $t_F = t_{R_{p0.2}}$. Marked (x) are impact points for instantaneous engine cut-offs at $t_{R_{p0.2}}$. The shaded areas represent areas which could be reached if the remaining fuel at $t_{R_{p0.2}}$ is used to accelerate the missile in an arbitrary direction.

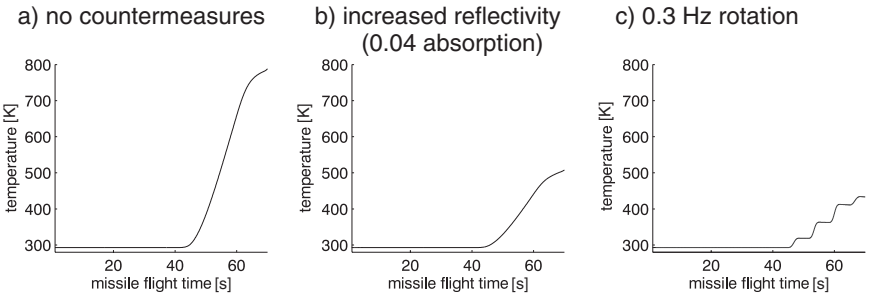

Figure 5: The effect of countermeasures on maximum temperature vs. flight time for the examined case study. Intensity distribution according to the case of reduced anisoplanatism and $t_{opt} = 60$ *s*. Plot b) shows the effect of a rotation along the missile's axis. Plot c) shows the effect of a missile surface with increased reflectivity.

effect of polishing. More practical would be last minute polishing, or a thin gold coating, which could decrease the absorption to a value as low as 1 percent[47] and is more resistant to environmental impact. A 0.1 mm gold coating would increase the mass of a 1.3 m diameter cylinder with a length of 15.5 m about 120 kg, decreasing the missile's range by roughly 30 km. A less expensive alternative would be copper, which has an absorption of 0.015 at the ABL's wavelength.[48]

Another countermeasure would be to rotate the missile around its axis, which would spread the laser energy over a larger area. The effect of a 0.3 Hz rotation is quite dramatic, as can be seen in Figure 5 c. Whether such a rotation is feasible depends on the guidance system of the missile. First generation guidance systems might not be able to achieve such a rotation. Both mentioned countermeasures could be combined which each other. In addition, there are other measures to insulate the missile from laser radiation, e.g., ablative coatings like cork.

Apart from these laser specific countermeasures, the usual offensive-defensive strategies come into play. The offense can try to overwhelm the defense by launching several missiles at once. Another option for the offensive would be to attack the ABL. As its platform is a Boeing 747, the ABL is highly visible and relatively vulnerable.

REVIEW OF ADDITIONAL ABL ENGAGEMENTS

In the course of the presented research, further ABL engagement scenarios have been analyzed. This includes missile defense scenarios including short range and intercontinental missiles and one scenario to assess an ABL application against a satellite in low earth orbit.

Short range missiles are more difficult to intercept than long range missiles, as a majority of their boost phase takes place in the lower atmosphere where absorption and turbulence are increased. As an example the case of a missile similar to a SCUD B flying from North Korea to South Korea was assessed, using the same distance between the launch pad and the ABL position as described in the detailed example in the last section. The parameters used for the assessment are shown in Appendix D. In the case of full anisoplanatism, the missile would be heated to about 80 K, which is not sufficient to significantly lower the yield strength of the wall material. Even for the assumption of reduced anisoplanatism, only at the end of the boost phase, stress levels reach the temperature dependent elastic limit. It is questionable whether the ABL could be used for such a scenario.

The situation is different for multi-stage intercontinental ballistic missiles. The influence of turbulence is less severe than for medium range and short range missiles, because the boost phase for an ICBM terminates at a higher

altitude. Scenarios including liquid-fueled ICBMs launched from North Korea, Iran and China have been assessed. The scenarios assume a missile launch in the middle of the countries and the ABL stationed 200 km from their respective coasts over the Sea of Japan, the Black Sea and the Yellow Sea, resulting in distances of 400 km, 900, km and 1600 km between the launch pad and the ABL. Using the same input data for the second stage as presented for the medium range missile (see Tables 2, 3 and 4 in Appendices A, B and C), the calculations for scenarios involving Iran and North Korea indicate that stress levels exceeding the yield stress can be induced in the boost phase of the second stage for both full anisoplanatism and reduced anisoplanatism. Please note, that this assessment depends on the same assumptions as presented in the appendix for the case of a midrange ballistic missile launched from North Korea to a target in Japan. However, in contrast to that case, for an ICBM the first stage already provides considerable acceleration before the second stage is destroyed. This implies that the impact point of the warhead will be several hundred kilometers from the launch pad. In addition, the third stage could still be activated, which would further expand the possible area of impact.

The scenario involving a launch in China would not allow for a successful intercept. The distance of approximately 1600 km implies that about 90 percent of the boost phase will have passed before the missile rises over the ABL's horizon and there is a line-of-sight between the ABL and the missile. At that point, the beam still has to pass through the lower atmosphere, which prevents the intercept.

Compared to the missile defense cases, the assessed anti-satellite scenario is considerably less challenging for the ABL. The ABL can maneuver to an ideal firing position directly below the satellite's trajectory, as satellite trajectories are highly predictable. Hence, the beam can be directed upwards and its passage through the lower atmosphere will be very short compared to all presented missile defense scenarios. For the calculations, the Hubble Space telescope was used as an example, as its setup has been published by NASA.[49] In addition, it is reportedly similar to that of a surveillance satellite.[50] The Hubble Space telescope is orbiting in an altitude of 550 km above the Earth's surface. Calculations show that during an ABL engagement the temperatures in the outer hull could exceed the melting point by more than 1000 K. Therefore, destruction is almost certain. Furthermore, countermeasures available to missiles may not be applicable to satellites. For example, due to the impact of micro debris, radiation and repeated circles of extreme temperature fluctuations, high reflective surfaces might lose their reflectivity in a space environment over time. In contrast to missiles, no last minute surface finish can be applied just before an laser attack. And while sensors could be protected by shutters, sensors would not be available as long as the shutter is in place.

CONCLUSION

Laser DEW development is progressing on two tracks. On the one hand, using available civilian technology and on the other hand focusing on high-power chemical lasers, which today have no civilian application. Both tracks have provided prototypes and testing is underway. Whether the deployment of laser DEW implies consequences for international security depends on the technical capabilities of these systems. This paper presented a physics-based assessment method for laser DEW engagements, using the U.S. Airborne Laser missile defense system as a case study.

Assuming an output power of 3 MW and engaged missiles with no countermeasures against a laser attack, the ABL could in principle be used against the examined type of mid-range and intercontinental liquid fuel missiles if they are launched from a small country like North Korea. This capability depends especially on the ABL's ability to correct for the negative effects of atmospheric turbulence on laser beam propagation. The successful implementation of an adaptive optics correction using a technology involving a distributed beacon on the casing of the targeted missile is crucial. It is disputed whether this is possible for the necessary distances of several hundred kilometers. In case the distributed beacon does not work, full anisoplanatism will occur. For full anisoplanatism the presented case of a liquid fuel missile with a range of 1000 km represents the cut-off for possible engagements, even for a small country like North Korea. The usability of the ABL would be restricted to missiles with more extended boost phases. In all presented cases, the intensity provided by the ABL is not sufficient to destroy warheads. Hence ABL engagements will result in a shortened boost phase of the starting missiles and in a shortened missile trajectory, but the laser will not destroy the warhead. In addition, the dense lower atmosphere prevents early ABL engagements, and for that reason in the assessed defensive scenarios the ABL is not able to disable missiles close to their launch pad and their warheads will cover distances of several hundred kilometers before impact.

The complexity of the presented analysis itself points out that a successful missile defense engagement depends on many factors, including both missile and laser parameters. For example, targeting still fueled tank sections of single-walled missiles would not be successful as the casing is cooled by the fuel. This is not true for double-walled, cryogenic missiles, but they might employ additional thermal insulation. Solid fueled missiles are in general more difficult to destroy by lasers than liquid fuel missiles, as elaborated by the APS study group. Therefore, details about the setup of the targeted missile have to be known. Introducing countermeasures could render the whole system useless.

Furthermore, recent congressional statements by the current Secretary of Defense indicate that the ABL might perform actually worse than described in this paper. R. Gates said that the ABL had to orbit inside North Korea or China in order to have capabilities for missile defense in a scenario involving North Korea.[51] This implies that the ABL program faces serious additional challenges with one or several of the ABL's components. This also implies that the defensive role for the ABL is very much restricted, as entering the airspace of a country like North Korea would naturally be highly provocative.

Finally, it was shown in this article that ABL engagements against satellites in low earth orbits are much easier to achieve than missile defense engagements. A deployment of the ABL could therefore be seen as a threat by other space faring nations leading to a new arms competition and to a proliferation of this technology. Preventive arms control measures negotiated before the deployment of laser DEWs worldwide would be a major step forward.

ACKNOWLEDGEMENTS

The article extends work done by the Jan Stupl during his dissertation,[52] which was conducted at the Institute for Peace Research and Security Policy at the University of Hamburg, Germany (IFSH), the Institute of Laser and System Technologies at Hamburg University of Technology (iLAS) and the Institute of Experimental Physics (IEXP) at the University of Hamburg between 2005 and 2008. The dissertation was supervised by Prof. Hartwig Spitzer (IEXP), Prof. Claus Emmelmann (iLAS) and Prof. Götz Neuneck (IFSH), who is also author of this paper.

The authors wish to thank Prof. Hartwig Spitzer and Prof. Claus Emmelmann for their longtime extraordinary support during the dissertation project. iLAS provided the lab environment for most of the conducted experiments. Additional experiments were conducted at the Bremer Institut für angewandte Strahltechnik (BIAS) in Bremen, Germany. Jan Stupl wants the thank the members of iLAS for providing a highly stimulating work environment and lots of personal support. He is also grateful to the Interdisciplinary Research Group on Disarmament, Arms Control and Risk Technologies (IFAR) at the IFSH for their input on the security implications and their personal support, as well as the Carl Friedrich von Weizsäcker—Centre for Science and Peace Research at Hamburg University.

The authors want to thank Scott Flagg, Harvey Lynch, Dean Wilkening and the anonymous reviewers for their helpful comments on earlier drafts of this paper. The authors are also grateful to Jürgen Altmann, Geoffrey Forden, Kate Marvel and Pavel Podvig for useful discussions.

Jan Stupl wishes to thank the Center for International Security and Cooperation (CISAC) at Stanford University for providing a highly stimulating work environment and for supporting this work.

APPENDIX A: CALCULATING INTENSITY ON TARGET

Introduction

A laser beam source at a given point $z = 0$ will deliver a certain output power P. The line-of-sight distance to the target is L. The energy is propagating along the path of the beam to a target at the point $z = L$, as illustrated in Figure 6. The altitude over sea level $h(z)$ may vary. Along this path, the intensity distribution in a plane perpendicular to the propagation path will change. A common way to describe these changes is to define a beam diameter. The beam diameter is usually defined as a certain threshold in intensity I in a given plane z_1.

In order to maximize the effects on a target, the usual approach is to focus the beam to the smallest possible beam diameter at the target location. A smaller beam diameter implies that more energy is focused on a smaller area. In any case, the minimum beam diameter is governed by the distance L between the laser and the target, the wavelength of the laser and the diameter of the employed optics. If the beam travels in the atmosphere, the intensity on target is further reduced. First, a fraction of the energy will be absorbed by the atmospheric path the beam is traveling through. Second, the beam diameter will not reach its minimum, as the beam divergence is increased by several effects, including atmospheric turbulence and laser performance. Both absorption and increased divergence depend on the path of the beam through the atmosphere, as absorption and turbulence depend on the altitude h. In general, this path can change during a laser DEW engagement. The following paragraphs describe the assessment of the different influences, first looking at the minimum beam diameter.

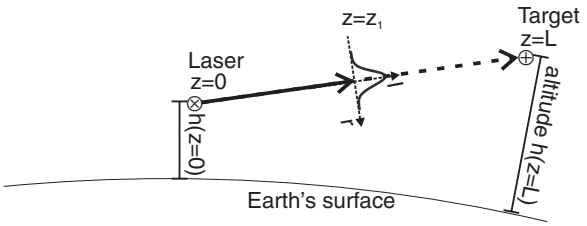

Figure 6: Illustration of the quantities used to calculate laser intensities *I*. The laser is located at $z = 0$ at an altitude $h(z = 0)$ above sea level. The target is located at $z = L$, L is the line-of-sight distance between laser and target. The altitude $h(z)$ above sea level may vary along the path of the beam through the atmosphere. At $z = z_1$, the intensity distribution perpendicular to the path of the beam is illustrated.

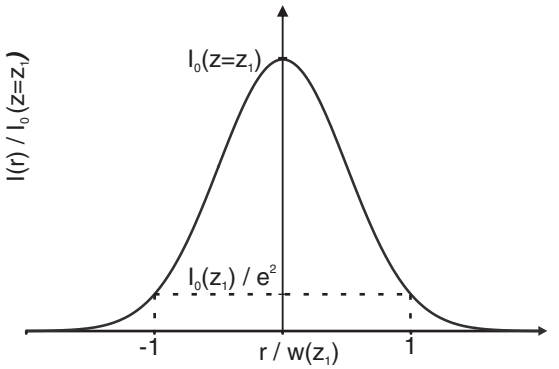

Figure 7: Intensity distribution of a Gaussian beam in a given plane $z = z_1$. The distribution is normalized with the maximum intensity $I_0(z_1)$, the distance r in that plane is normalized with the beam radius $w(z_1)$ at $z = z_1$.

Minimum Laser Beam Diameter for Vacuum Beam Propagation

Propagating laser beams can be described using the concept of Gaussian beams.[53] To simplify the proceeding at this point, an axial symmetric intensity distribution in the direction of the beam propagation is assumed, which occurs if circular optics are used inside the laser. As illustrated in Figure 7, there is a maximum intensity I_0, which defines the center of the beam. The distance r where the intensity drops to less than 14% of the maximum value in a given plane $z = z_1$ is called the beam radius $w(z_1)$. During beam propagation, the beam radius is not a constant, as illustrated in Figure 8. The minimum beam radius w_0 is reached at the focal plane. Using the concept of Gaussian beams, the minimum beam diameter at a given distance L from a focusing element with a diameter D can be calculated, as shown by Siegman.[54] It is assumed, that the beam diameter at the position of the focusing element is adjusted in such a way that less than one percent of the beam energy is lost because it is

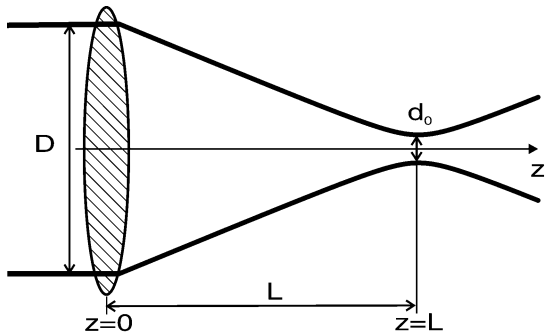

Figure 8: Minimum focal diameter d_0 of a laser beam in a distance L. D is the diameter of the focusing element.

overshooting the lens. The minimum beam radius then results to

$$w_0 = \frac{\lambda L}{D}. \tag{1}$$

For the case of the ABL, which employs a mirror with 1.5 m diameter and is using a COIL with a wavelength of 1.3 μm, Eq. (1) results in a minimum focal diameter of about half a meter in distance of 300 km.

Assuming the minimal focus diameter, the circular intensity distribution on a target in a distance L computes to

$$I(L, r) = \frac{2P}{\pi w_0^2} \exp\left(\frac{-2r^2}{w_0^2}\right). \tag{2}$$

In this equation, r is the distance from the beam center in the plane $z = L$ and P is the output power of the laser.

In addition to the beam diameter, the intensity is also influenced by the angle of incidence on the target and atmospheric losses. As illustrated in Figure 9, in a case of a grazing beam incidence, the same power is distributed over a bigger target area than for perpendicular incidence, resulting in a smaller intensity. For a laser beam with an axially symmetric intensity distribution, the effects can be accounted for by two angles, α and β. The angle α is the angle between the laser beam and the missile's velocity vector. The angle β depends on the aim point. As the missile has a cylindrical shape, it can be chosen in such a way that for a given time t_{opt} β equals 90 degrees. Depending on the missile's trajectory, tracking that aim point can result in a variation of both angles during the engagement. For now it is assumed that the missile is not rotating around its axis.

For the case of missile defense using the ABL, the beam will propagate through the atmosphere and Eq. (2) has to be adapted to incorporate

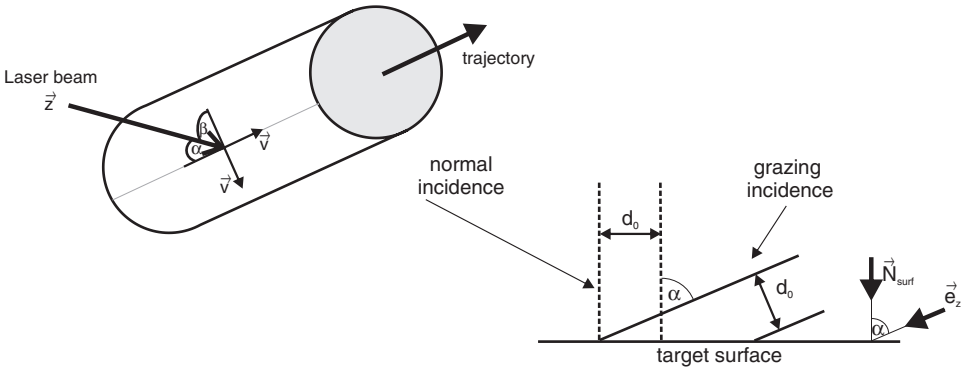

Figure 9: Effect of angle of incidence on intensity. In case the beam is not parallel to the target's surface normal $\vec{N}_{surf}$, the beam will spread over a larger area and the effective intensity will be smaller.

absorption, increased divergence and the angle of incidence. This is done by using the angles α and β as well as two additional parameters, the atmospheric transmittance τ and the Strehl ratio:

$$I(L,r) = \cos(\alpha)\cos(\beta) S_{\text{sum}} \tau \frac{2P}{\pi w_0^2} \exp\left(\frac{-2S_{\text{sum}} r^2}{w_0^2}\right). \tag{3}$$

The atmospheric transmittance τ accounts for the real energy losses due to scattering and absorption. The Strehl ratio S_{sum} accounts for all effects which reduce the intensity due to a larger than ideal beam radius. The Strehl ratio is defined as:

$$S = \frac{I_{0\text{real}}(z)}{I_{0\text{ideal}}(z)}. \tag{4}$$

In reality, propagation through turbulence might result in a non Gaussian intensity distribution in the target plane. In that case, Eq. 3 will only be an approximation. However the introduction of the Strehl ratio insures that the calculated maximum intensity is still correct.

In order to calculate it, a range of different effects are accounted for by individual Strehl ratios. These individual Strehl ratios are cumulated using Eq. 5, which is in good agreement with experimental results quoted in the literature.[55]

$$S_{\text{sum}} = \frac{1}{1 + \sum_i \left(S_i^{-1} - 1\right)}. \tag{5}$$

Apart from atmospheric effects, one individual Strehl ratio accounts for the discrepancy between real laser beams and ideal Gaussian laser beams. Real laser beams do not necessarily follow the Gaussian distribution illustrated in Figure 7, which ultimately results in a higher beam divergence. Nevertheless, the propagation laws of Gaussian beams still apply, if a beam quality factor is introduced to account for the increased divergence, as Siegman has shown.[56] This beam quality factor can be translated into a Strehl ratio.

The following paragraphs will describe the atmospheric effects in further detail. First, the assessment of atmospheric absorption and scattering is described, followed by an assessment of atmospheric turbulence on the Strehl ratio.

Intensity Reduction Due to Atmospheric Absorption and Scattering

Atmospheric absorption and scattering reduces the power propagated by the laser beam. This reduction is accounted for by incorporating transmittance

τ into Eq. 2. The transmittance τ is derived by the Beer-Lambert law

$$\tau = \exp\left[-\int_0^L \alpha(z)\mathrm{d}(z)\right], \tag{6}$$

where $\alpha(z)$ is the local absorption coefficient, which is integrated along the path of the beam. The local absorption coefficient is a cumulative factor, including absorption on the molecular and atomic level, as well as scattering on the atmospheric constituents, including aerosols:

$$\alpha(z) = \sum_i \alpha_\mathrm{i}(z). \tag{7}$$

The factors $\alpha_\mathrm{i}(z)$ depend on the local density of the constituent i, the temperature and pressure, as well as the wavelength of the propagating laser beam. For high intensities, non-linear effects set in, in which case α becomes a function of beam intensity, too. In the presented case studies, such intensities are not reached.

Scattering and absorption are effects which happen on a quantum level, single photons will be removed out of the laser beam on a statistical basis. Therefore, the beam diameter itself is not affected, only the total power P, which is propagated along the beam. There is no analytic solution to determine τ, but numerical approaches have been developed in the past. In the presented research, the software MODTRAN 4 was used. MODTRAN is a standard tool in atmospheric physics.[57] MODTRAN incorporates atmospheric models to describe the distribution of the atmospheric constituents at different altitudes, a spectroscopic database to allow to calculate wavelength dependent absorption, as well as the algorithms to calculate the transmittance of different propagation paths. Figure 10 shows an example of a MODTRAN result for the visible and near-infrared wavelength spectrum. For the wavelength of the ABL's high energy laser (1.3 μm), and a 100 km path at an altitude of 12 km there is a transmittance of 96 percent. For a path starting out at 12 km altitude and reaching the ground in a distance of 100 km there is a transmittance of 22 percent. Both values are valid for a clear sky with no clouds or rain. Calculations including rain in the path of the beam result in a 100 percent absorption or zero percent transmittance.

This implies that atmospheric absorption can have a significant effect for possible missile defense applications, especially during the early boost-phase, when the missile is close to the ground. At an altitude of 12 km the ABL is above the influence of weather most of the time, so the effects are less significant for ABL engagements in those cases. Nevertheless, thunderclouds have been observed up to an altitude of 20 km,[58] which would prohibit beam transmission. For calculations in the presented case study, a clear sky without rain is assumed. This is done in order to allow for a best-case study of the ABL's abilities.

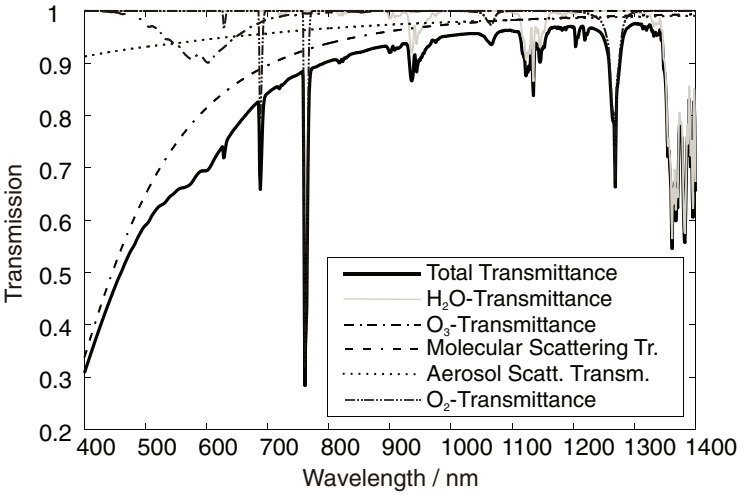

Figure 10: MODTRAN calculation of transmittance for a 100 km path at 12 km altitude, using the U.S. Standard atmosphere, no clouds or rain at rural aerosol distribution with 23 km meteorological visibility (VIS) at ground level.

Intensity Reduction Due to Uncompensated Turbulence

While atmospheric absorption and scattering are reducing the intensity on target by reducing the total transmitted power, the effects of turbulence diminish the intensity by increasing the diameter of the focused beam. Turbulence leads to local changes in index of refraction along the path of the beam. As turbulence effects vary with time, the effect is comparable to the encounter of an distorted lens with changing optical properties. A visible result of this effect is the flickering of stars in the night sky. The light is refracted differently over time, and on the ground the star seems to be moving. This effect is called tilt or jitter and is the lowest order optical effect of turbulence. In addition, the beam encounters phase deviations, which lead to higher order optical aberrations, for example a defocusing effect.[59] Severe turbulence might even break up the beam in several smaller spots.

The effects of turbulence are more severe near the ground than at higher altitude. Hence the effective range of a laser weapon will depend on the altitude of the laser and the engaged target. Missiles that are reaching the end of their boost phase are an easier target than shortly after launch.

Turbulence can be treated as a statistical problem according to Richardson and Kolmogorov.[60] It induces fluctuations in the local index of refraction n. In order to quantitatively assess the effects of turbulence on laser beam propagation, turbulence statistics are incorporated into electromagnetic wave propagation calculations. In a distance s from a point $\vec{r}$ the average change in the index of refraction $< [n(\vec{r}+\vec{s}) - n(\vec{r})]^2 >$ can be accounted to the distance s and a single parameter $C_n^2(\vec{r})$, called the structure parameter.[61] As specified in Eq. 8, the index of refraction between the point $\vec{r}$ and $(\vec{r}+\vec{s})$ varies on average

by $n^2(\vec{r}) \cdot s^{2/3}$, if the distance s is in the range between l_0 and L_0:

$$< [n(\vec{r}+\vec{s}) - n(\vec{r})]^2 >= C_n^2(\vec{r}) \cdot s^{2/3} \ , \quad \text{if } \ l_0 < s < L_0. \tag{8}$$

The boundaries l_0 and L_0 vary with atmospheric conditions and are in the order of a few millimeters for l_0 and several meters to about a hundred meters for L_0.[62] $C_n^2(\vec{r})$ varies in altitude, and depends on geographic and seasonal influences. It also depends on the time of day and is subject to the weather. In order to allow for an assessment of turbulence on optical propagation, several models for the average behavior of C_n^2 in different altitudes h have been devised in the past. The ABL is designed to work in turbulence twice as strong as predicted by the model CLEAR I Night.[63] This seems to be a somewhat arbitrary choice, as C_n^2 measurements show variations between one and two orders of magnitude during the time of day alone.[64] In addition, the validity of CLEAR I Night is disputed, because the model was devised during nighttime measurements over the desert of New Mexico and actual turbulence in real operational scenarios might be increased.[65] However, as 2 × CLEAR I was also used by the APS study group on boost phase missile defense, this research also uses this assumption in order to deliver comparable results. Please refer to Figure 28 in Appendix D for an illustration of the dependence of C_n^2 on altitude according to CLEAR-1 and the model algorithm.

The predicted fluctuations are incorporated in the wave equation using a first order perturbation approach, called the Rytov approximation. The Rytov approximation is valid for the case of minor turbulence, as is expected at the ABLs altitude. For a detailed description of the application of the theory especially for the assessment of the ABL, please refer to the APS study on boost-phase missile defense.[66] For a short introduction into optical turbulence, please refer to the publications of Andreas, Tyson or Smith.[67] Detailed information can be found in the publications of Sasiela and Strohbehn.[68]

In order to evaluate the effects of turbulence, path integrals along the propagation of the beam are solved, as illustrated in Figure 6. A measure for global turbulence along the path of the beam is the Fried's coherence length r_0 and the Rytov variance σ_{R}^2:

$$r_0 = \left[0.423k^2 \int_0^L C_n^2(h(z)) \left(1 - \frac{z}{L}\right)^{5/3} \mathrm{d}z \right]^{-3/5}. \tag{9}$$

$$\sigma_{\mathrm{R}}^2 = 0.5631k^{7/6} \int_0^L C_n^2(h(z)) \left[z \left(1 - \frac{z}{L}\right) \right]^{5/6} \mathrm{d}z. \tag{10}$$

Using the Fried parameter r_0, Sasiela has derived an asymptotic series to calculate the Strehl ratio after encountering of turbulence[69]

$$S \approx \left(\frac{r_0}{D}\right)^2 - 0.6159 \left(\frac{r_0}{D}\right)^3 + 0.05 \left(\frac{r_0}{D}\right)^5 + 0.00661 \left(\frac{r_0}{D}\right)^7 \pm \ \cdots \quad \text{for } D > r_0. \tag{11}$$

For the ABL the optic diameter D is 1.5 m, its cruising altitude is quoted to be 12 km. For a beam starting at 12 km and going directly into space, Eq. 11 computes to 0.44 if turbulence according to 2 $\times$ CLEAR I night turbulence is used. So the maximum intensity is diminished by more than 50 percent. For a path travelling 100 km at an altitude of 12 km, the Strehl factor computes to 0.08, therefore in this case the peak intensity is less than 10 percent compared to vacuum propagation. This decrease is a result of higher turbulence at low altitudes. If turbulence according to 10 $\times$ CLEAR I is used, the resulting Strehl ratios are 0.1 and 0.01 respectively.

Equation 11 implies diminishing Strehl factors with increasing optic diameters D. This occurs because with increasing beam diameter, more turbulence cells with different optical properties will appear in the path of the beam. Hence, for the case of atmospheric propagation, the maximum intensity on a target can only be increased up to a certain limit by increasing the optic's diameter.

Adaptive Optics and Its Limits

For that reason, the useful diameter of the focusing optics of a laser weapon is limited in its size, if no further measures are taken. The same is also true for astronomic telescopes on the ground. It was first suggested in astronomy to use so called adaptive optics to overcome the effects of turbulence. As atmospheric turbulence is working like a distorted lens, its effects can be compensated with another optical element. The corrective element has to be adaptive as the turbulence effects vary in time, hence the term adaptive optic.

In astronomy, the light of a bright star is employed to measure the phase deviations of the incoming light waves.[70] A computer system is calculating the necessary changes to the optical system in real time. Jitter is commonly compensated using a fast steering mirror. Higher order phase distortions are corrected using a deformable mirror, where a set of actuators are deforming its surface locally for fractions of the wavelength of the incoming light. For a laser DEW, the same working principle applies. Instead of using the light of a bright star, a section of the target is illuminated by a so called beacon laser. The returning light from this beacon is used to measure the phase distortions for that path through the atmosphere. The optics are pre-distorted in order to correct for the distortions the beam is going to encounter. The performance of such an adaptive optics system is limited by the resolution of phase and tilt measurements, the number and accuracy of actuators, the quality of the employed algorithms and the effective bandwidth of the entire system.

The ABL's adaptive optics setup has been tested before the start of its implementation and the results have been published.[71] The APS study group on boost phase missile defense compiled the results and published a relationship between the Rytov variance and the expected Strehl ratio of the system.[72] This

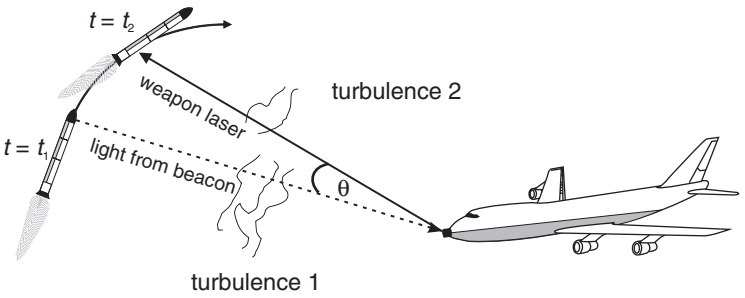

Figure 11: Anisoplanatism: The ability to correct for turbulence is limited if the light of the beacon does not pass through the same path as the weapon laser. The light from the beacon will leave the missile at the time $t = t_1$, the weapon laser will reach its aim point at $t = t_2$, while the aim has been corrected for the missile movement. Subject to missile speed, the range and the speed of light, a significant angle θ can develop between the path of the beacon and the path of the weapon laser.

relationship is valid if the light from the beacon travels through the same path as the high energy laser beam. It is used in this paper to calculate the Strehl ratio representing the adaptive optics performance.

For a path in a 2 × CLEAR I atmosphere, starting from 12 km altitude and going directly into space, it results in a Strehl ratio of 0.88, nearly doubling the intensity compared to the uncompensated case without adaptive optics. For a 100 km path at 12 km altitude, the resulting Strehl ratio is 0.42, resulting in a fivefold increase compared to the uncompensated case.

However, these results only apply if the light from the beacon travels through the same path of air as the high energy laser beam. If the ABL is targeting a fast moving missile, there is a natural limit which prevents such a scenario: the finite speed of light c. Suppose the adaptive optics system is receiving the turbulence information from an illuminating beacon on the tip of the missile at the time $t = t_1$, as illustrated in Figure 11. If the distance to the ABL is 300 km and the missile is moving with a speed of 6 km/s, it will have moved 12 m when the actual high energy laser weapon beam is hitting the missile. The tracking system of the ABL could compensate for that movement to hit arbitrary aim points on the missile, but if the chosen aim point is higher or lower than the calculated 12 m, the actual high energy laser beam would travel through a different path of air than the light from the beacon. As illustrated in Figure 11 an angle θ between the path of the high energy laser beam and the path of the beacon appears for those cases. One speaks of anisoplanatism, as the two paths are not the same anymore. A degradation of the adaptive optics correction results in that case.

Turbulence cells appear in sizes in the order of centimeters up to a hundred meters. Their size generally increases with altitude. Turbulence will vary accordingly. Near the ground, an offset of 12 m will therefore be significant, where at high altitude this might not be the case. In general, the so called

isoplanatic angle θ_0 is used to assess the significance of the effect. It is calculated by integrating turbulence along the path of the beam, as specified in Eq. 12. Segments of the beam outside the atmosphere will not contribute, as C_n^2 is zero in vacuum.

$$\theta_0 = \left[2.914 k^2 \int_0^L C_n^2(h(z)) z^{5/3} \mathrm{d}z \right]^{-3/5}. \tag{12}$$

If the actual angle θ is greater than θ_0, a significant degradation of the adaptive optics performance can be expected. The Strehl ratio S_θ accounts for this effect. It is calculated using the actual angle θ and the isoplantic angle θ_0:

$$S_\theta \approx \exp\left[-\rho_{\mathrm{op}} \left(\frac{\theta}{\theta_0} \right)^{5/3} \right]. \tag{13}$$

The factor ρ_{op} is accounting for the fact that not all optical aberrations influence the intensity on target. For example, the addition of a constant phase to the wavefront has no effect on the intensity. Further details are described in detail by Barton et al.[73] and Stroud.[74]

The actual value of the angle θ strongly depends on the details of the engagement.

For example, let us assume a missile traveling with a speed v_1 at the time t_1. In order to use the same path for beacon and high energy laser beam (and hence avoid anisoplanatism), the missile has to be targeted at a point in a distance $d_1 = 2Lv_1/c$ from the beacon, as illustrated in Figure 12 b. A limit to this approach is the missile length. If the missile is shorter than d, there will always be anisoplanatism. If d is smaller than the missile length, it implies an aim point on the missile, but whether that is vulnerable to a laser attack is not certain.

Another challenge is the changing speed v of the accelerating missile. If v is different from v_1, also d will differ from d_1. However, in order to heat up one point on the missile as fast as possible, the aim point has to be fixed and

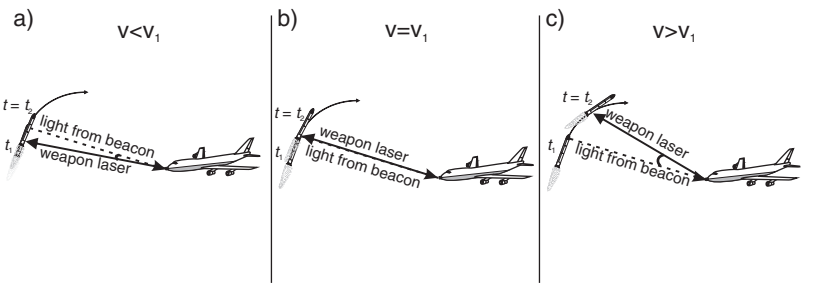

Figure 12: Anisoplanatism effects depend on the missile speed *v*. If the aim point and the beacon on the missile are fixed, only at one speed $v = v_1$ will the path of the beacon and the path of the weapon laser match.

cannot change with changing missile speeds, as changing the aim point would imply spreading out the energy along the length of the missile. If beacon and aim point are fixed points on the missile, anisoplanatism will appear as soon as v differs from v_1, as illustrated in Figure 12. For $v = v_1$, there is no anisoplanatism. If $v > v_1$, for the point d anisoplanatism cannot be avoided, as there is no way to place a beacon higher than the missile's tip.

For $v < v_1$ there are approaches to reduce anisoplanatism. One is to *vary the position of the beacon* during the engagement, another is to *use turbulence information already gathered* during earlier measurements.

Varying the position of the beam: Moving the beacon away from the tip of the missile and along the missile implies two major challenges: First, correcting for tilt will be more difficult, and second the beacon will no longer be a point source.

To correct for tilt, a sharp edge is needed to provide a point of reference. Moving the beacon down from the tip would imply losing that information. In order to allow for tilt compensation and still to move the beacon, the ABL will use two different beacon lasers, one laser for higher order corrections, called the Beacon Illuminator Laser (BILL) and one for tilt correction, called the Tracking illuminator Laser (TILL).[75] Therefore, using this approach, only higher order modes can be corrected with reduced anisoplanatism if a movable beacon is used, but not tilt, as the TILL is still fixed at the missile's tip. So called tilt-anisoplanatism remains.

While the illuminated tip will approximately act like a point source, the BILL placed on the missile's body will be distributed over a large area, which minimum size is determined by Eq. 1, but which actual size will be much bigger than that, as the beacon is not compensated for turbulence. As the missile's surface does contain a certain roughness, this roughness will introduce phase distortion on its own. The result is that the beacon in this case will be incoherent as well as distributed. Phase measurement will not be straightforward, and the performance of turbulence corrections using such a beacon is disputed.[76]

Using already gathered turbulence information: To avoid tilt-anisoplanatism, the second approach can be implemented. The tip, and hence the TILL's beacon will already have passed a certain point in the atmosphere, before the chosen aim point is arriving there. If information from this point already has reached the ABL, this "old" turbulence information can also be used. The challenge involving this approach is that there is a delay between the gathering of the information and the application of the correction. During this delay, the atmosphere might not change that much, but the ABL itself is moving to a different position, as illustrated in Figure 13. Hence, while the path of the high energy laser will coincide with the position of the beacon at the missile, at the position of the ABL, the path will have been shifted. Hence, a so called "delay anisoplanatism" appears. It is caused by wind speed and aircraft movement rather than missile movement.

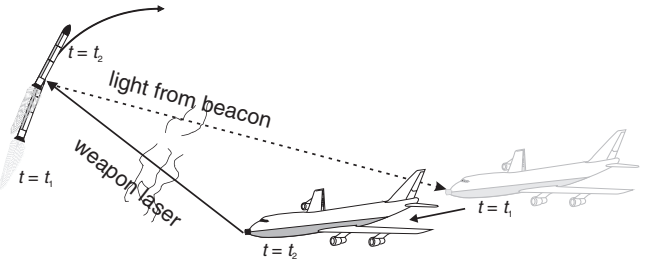

Figure 13: Effects of using old turbulence information for adaptive optics turbulence correction. The aircraft movement will introduce a so called "delay anisoplanatism," even if the atmosphere at the aim point has not significantly changed between turbulence measurement and the propagation of the weapon laser.

Barton et al. calculated the phase difference for this scenario.[77] Using their results, the Strehl ratio S_{del} introduced by a time delay Δt and a wind speed v_w computes to

$$S_{\mathrm{del}} = \exp\left(-1.58 \cdot \left(\frac{v_w \Delta t}{r_0} \right)^2 \cdot \left(\frac{r_0}{D} \right)^{1/3} \right) \tag{14}$$

The wind speed v_w is the cross wind perpendicular to the beam, resulting from aircraft movement and real wind in the different layers of the atmosphere. The cruising speed of a Boeing 747-400 is in the order of 250 m/s[78] and the beam will be most likely perpendicular to the flight path.[79] Therefore real wind speed[80] is only a minor effect and has been neglected in this analysis. Instead the velocity of aircraft is assumed to be equal to the cross wind.

Intensity Calculations for the Presented Case Study

The intensity on target will depend in large part on the adaptive optics performance. As it is not clear how well the distributed beacon of the ABL adaptive optics system will perform in a real scenario, two different cases have been investigated.

Full Anisoplanatism

In this case, it is assumed that the complete turbulence information is gathered from a beacon on the tip of the missile. A certain aim point can only be targeted with minimal anisoplanatism for a short amount of time, as the changing missile speed will induce an increasing angle θ between the path of the beacon and the path of the high energy laser beam, resulting in anisoplanatism.

Reduced Anisoplanatism

Here it is assumed that the combination of the ABL's beacon and tracking lasers BILL and TILL is working perfectly. As long as the missile speed

$v < v_1$ (compare Figure 12), the BILL can be placed sufficiently higher than the aim point on the missile. Higher order distortions do not appear, only tilt. Tilt anisoplanatism is reduced as much as possible by using already gathered turbulence information. Hence, for $v < v_1$, only time delay anisoplanatism remains.[81] For $v > v_1$ full anisoplanatism sets in.

In addition, the intensity strongly depends on the choice of aim point. For example, if the aim point was the missile's tip, full anisoplanatism would set in at once, as it is not possible to place a beacon higher than that. To analyze the effects of different aim points, this chosen aim point is described in terms of an **optimal engagement time $\mathbf{t_{opt}}$** below. At the flight time t_{opt}, the aim point is chosen so that anisoplanatism is minimal, usually in a distance $d = 2 \cdot L(t_{\mathrm{opt}}) \cdot v(t_{\mathrm{opt}})/c$ from the tip, or at the lower end of the missile if d is larger than the missile. At all other times, there will be different levels of beam degradation by anisoplanatism.

Table 2 summarizes further input parameters for the assessed scenario. Please note that the actual output power of the ABL's main chemical laser is classified, the official statement is that it is a "megawatt-class" laser.[83] The assumed value of 3 MW has been published in the 2003 issue of Jane's Electro Optical systems and has disappeared in the following editions.[84] As the APS study group also used that value, it was decided to do accordingly, to allow for comparable results.

Apart from Strehl factors introduced by the general adaptive optics performance and the effects of anisoplanatism, there are two further contributing factors. First, even the chemical laser employed in the ABL is not an ideal laser in a Gaussian sense. The ABL specifications translate into an additional Strehl factor of 0.69.[85] Second, the ABL's own movement through the air is introducing a boundary layer with high turbulence at the window, where the laser beam is leaving the aircraft. This local turbulence equates to a Strehl factor of 0.8.[86] The accumulated Strehl factor, including general adaptive optics performance and anisoplanatic effects, is calculated using Eq. 5.

Please note that for any real engagement, other factors might impair the ABL's performance and further reduce the laser intensity placed on the target. Target detection, discrimination and tracking over distances of several hundred kilometers are some additional challenges. For example, in order to point the laser beam at a certain aim point with an accuracy of half a meter over a distance of 400 km, the angular pointing accuracy of the steering mirror has to be in the order of 10^{-6} radians, while the optical setup is placed in a moving aircraft. As this article follows a best case analysis, it is assumed that those challenges can be overcome.

Figures 14 to 16 present the results of the calculations for the case study illustrated in Figure 3. Figure 14 a) and b) illustrate the details of the missile's trajectory. The steep increase in missile velocity during the 70 s boost phase is a potential source of strong anisoplanatism. The following diagrams are limited

Table 2: Input parameters for intensity calculation

ABL		Atmosphere		Missile	
Output power P	3 MW	Turbuence	2 $\times$ CLEAR I- Night	Boost phase	70 s
Wavelength λ	1.315 μm	Constituents	US Standard (1976)	Trajectory details	see Appendix D
Optic diameter D	1.5 m	Aerosols	rural with VIS = 23 km	Length	15.5 m
S_{window}	0.8	Season	Spring/Summer		
$S_{\text{beam quality}}$	0.69				
Aircraft altitude	12 km				
Aircraft speed	250 m/s				
Adapt. Opt. Performance	Barton et al.[82]				

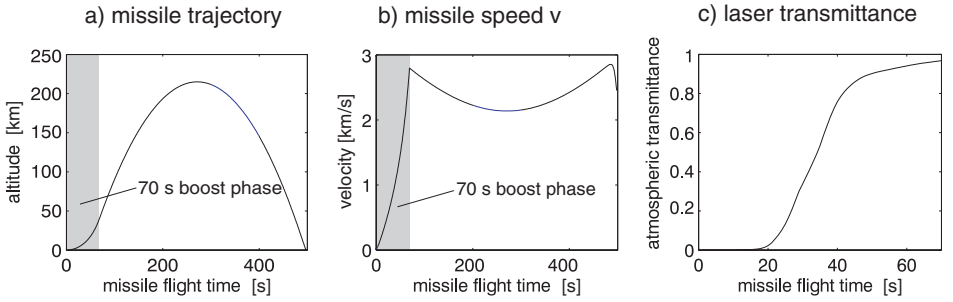

Figure 14: Time dependent trajectory parameters and atmospheric transmittance for the examined case study. Transmittance (Figure c) is shown for the boost phase only and changes significantly as the missile gains altitude.

to the boost phase only, as the ABL aims to destroy missiles during that time. Figure 14 c) shows the development of the laser transmittance during the boost phase. The lower atmosphere is strongly absorbing and about 20 s of the boost phase have to pass before significant transmittance can be achieved. A destruction of the missile on its launch pad is not possible for this reason alone.

Figure 15 shows the resulting maximum intensities on the target for different cases of anisoplanatism. Plot a) shows the maximum intensity's variation during the flight time, if anisoplanatism is neglected. The steep increase near the end of the boost phase is caused by a drop in turbulence at higher altitudes. Plot b) and c) illustrate the case of full anisoplanatism for different aim points, represented by the choice of optimal engagement time t_{opt}. Because of the changing missile speed, the maximum intensities can only be sustained for a short time interval around t_{opt}, before anisoplanatism becomes a significant factor.

Plot d) illustrates the case of reduced anisoplanatism by a perfectly working BILL and TILL combination onboard the ABL. If the challenges involved in the distributed beacon can be overcome, for flight times before $t_{\mathrm{opt}} = 60$ s the movable beacon will prevent anisoplanatism for all higher order distortions. Remaining is tilt anisoplanatism, in this case caused by time-delay. For $t > t_{\mathrm{opt}}$, the chosen aim point is above d. In this case, even if both beacons are placed on the tip of the missile, full angular anisoplanatism is unavoidable and therefore plots c) and d) resemble each other after $t > 60s$.

A comparison between plots b) and c) of Figure 15 highlights the importance in the choice of an aim point in regard to adaptive optics performance. In order to allow for a more comprehensive analysis of the resulting effects, Figure 16 plots the maximum energy per area which can be delivered during the boost phase against the optimal engagement time t_{opt}. The data have been derived by integrating maximum intensities (as they are shown for $t_{\mathrm{opt}} = 60s$ and $t_{\mathrm{opt}} = 40s$ in plots b) and c) of Figure 15) during the entire boost phase for a range of different aim points. In general, the delivered energy can be

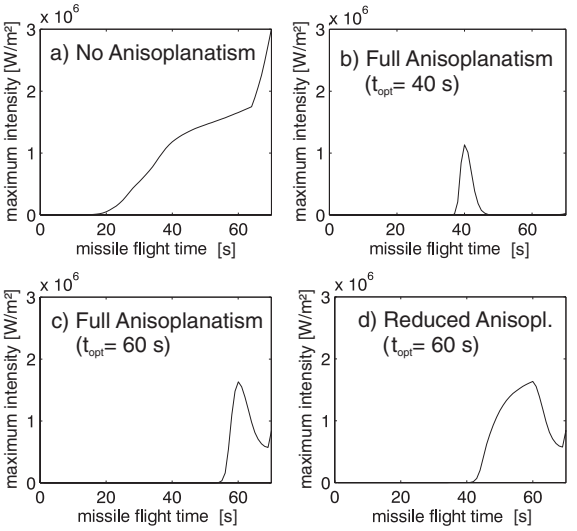

Figure 15: Calculated maximum achievable laser intensities on the target for different cases of anisoplanatism for the examined case study during the missile's boost phase. a): no anisoplanatism, turbulence is measured perfectly and corrected to the best abilities of the ABL's adaptive optics. The intensity is subject to diffraction, atmospheric transmittance and general adaptive optics performance. b) and c): full anisplanatism, only for two different optimal engagement times (40 s and 60 s respectively), turbulence is measured perfectly, for all other times during the boost phase, anisoplanatism reduces adaptive optics performance. d): reduced anisoplanatism: maximum intensity for the case of a perfectly working combination of TILL and BILL tracking and beacon lasers onboard the ABL. The beacon's position at the missile is not fixed.

maximized if the aim point is chosen for a time t_{opt} near the end of the boost phase, as the missile has reached a higher altitude with lower turbulence at that time. However, the delivered energy drops, when the target missile approaches the very end of the boost phase, as the remaining time to irradiate the target also gets shorter.

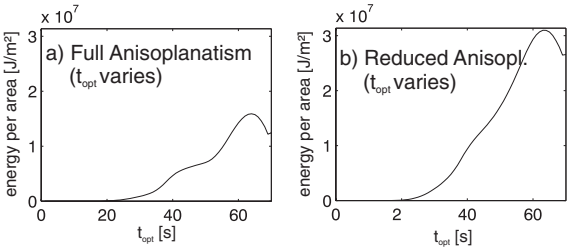

Figure 16: Maximum Energy per area delivered during boost phase dependent on the optimal engagment time t_{opt}. The calculated maximum intensities are integrated over the entire boost phase for different times t_{opt} of minimum anisoplanatism, hence different aim points. a) shows the case of full anisoplanatism, b) shows the case of reduced anisoplanatism, where the beacon's position is not fixed.

For the following temperature calculations, both the case of full anisoplanatism and reduced anisoplanatism are reviewed, as it is uncertain whether the ABL will be able to achieve perfect turbulence correction using the distributed BILL beacon. For both cases, the aim point according to $t_{opt} = 60$ s has been chosen. For that choice, 90 percent or more of the maximum energy per area can be deposited, as plotted in diagrams a) and b) of Figure 16. A further delay would only marginally increase the deposited energy, but might result in extended missile ranges, as the missile's acceleration increases at the end of the boost phase. That would indicate that, whatever other effects the laser might have, the missile or its debris gets closer to the planned target.

However, the choice $t_{opt} = 60\ s$ and the corresponding aim point is somewhat arbitrary at the moment and the effects of this choice will be examined later. With that choice, the achievable intensity distribution is now defined for the entire boost phase. The choice of the aim point also defines the angle of incidence on the missile. Using this information, the temperature increase at the target is calculated.

APPENDIX B: CALCULATING TARGET TEMPERATURE

Introduction

Calculating the temperature in a target requires knowledge about its composition. A single-stage liquid fuel missile consists of a warhead section on top, fuel tanks in the middle and an engine section, as illustrated in Figure 17 a). Multi-stage missiles combine multiple tank and engine sections. In general, all sections of the missile, including the warhead and the engine, could be targeted by the ABL. As was shown in the last section, the position of the aim point might be restricted by the effectiveness of the turbulence corrections, and especially by the effects of anisoplanatism. In addition, the vulnerability of the different missile portions is important.

For the presented case study, the maximum laser intensity on the missile's surface is smaller than 300 W/cm^2. Only part of this intensity will be absorbed in the irradiated surface and converted into a surface heat flux. In contrast to that, a warhead re-entering the atmosphere at the end of its trajectory is encountering a heat flux of an order of magnitude of 2000 W/cm^2.[88] For that reason, warheads are reinforced with a thermal insulation, designed to withstand such a heat flux. The engine is mostly covered by an external wall and also designed for high temperatures, therefore, the laser in this scenario will not have a significant impact if aimed on the warhead or the engine. Hence this assessment concerns the scenario of a targeted fuel tank.

As shown in the pictured Iraqi Al Samoud-2 missile, the outer wall of the tank is identical to the outer wall of the missile and hence a structural element.

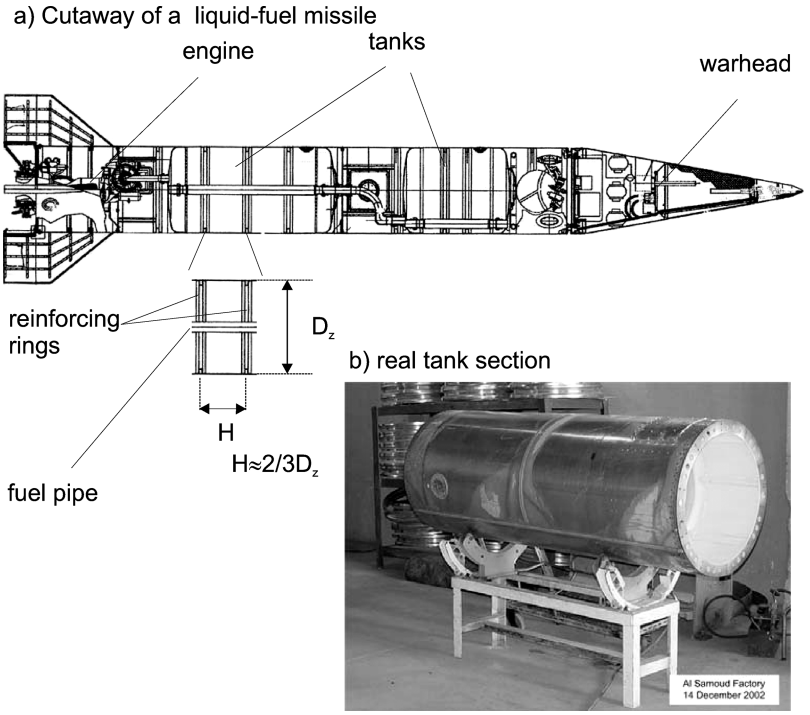

Figure 17: Makeup of a liquid fuel missile. Adapted source: UNMOVIC compendium.[87] The distance *H* between two reinforcing rings is approximately two thirds of the diameter D_z.

While Iraqi missiles might not be relevant today, the general setup of liquid fuel missiles of states like North Korea or Iran is very similar to this.[89] Therefore, the following damage assessment is reduced to the laser irradiation of a hollow cylinder.

Assessment Method

Figure 18 shows the setup of the thermo-physical problem. The laser beam is irradiating the outside of the wall of the cylindrical tank. For this case only temperatures below the melting point are of interest, because melting would indicate a destruction of the missile. Hence, there are no heat sinks or sources in the interior of the wall and the temperature T(x,y,z,t) inside the volume of the irradiated wall is governed by the heat equation

$$\rho c_{\mathrm{p}} \frac{\partial T(x,y,z,t)}{\partial t} = \mathrm{div}(\kappa\ \mathrm{grad}(T(x,y,z,t))), \tag{15}$$

where C_{p} is the heat capacity, κ is the thermal conductivity and ρ is the density of irradiated material. To solve this differential equation, initial and boundary conditions are set to account for the given scenario. The initial condition is a

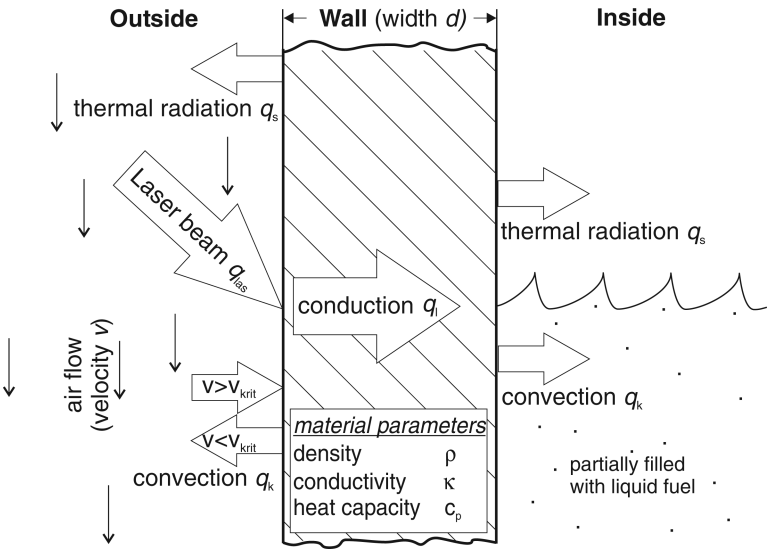

Figure 18: Problem setup for temperature calculations in a missile body. A schematic cutaway of a fuel tank's wall and the appearing heat sources and heat sinks are shown. The missile's movement through the atmosphere translates into an airflow on the outside boundary. Depending on the missile's velocity *v*, this airflow can either act as a convective heat sink or heat source. The inside is partially filled with a decreasing fuel supply.

temperature distribution at the beginning of the laser irradiation, the boundary condition is the cumulated heat flux q at any given point of the surface of the wall,

$$q(\vec{r}, t)|_{\vec{r}\ \epsilon\ \text{surface}} = \sum q_i. \tag{16}$$

Possible heat sources q_i are the absorbed laser energy $A \cdot I(x, y, z, t)$ and air friction, if the missile is moving through the atmosphere with a velocity exceeding the speed of sound. Heat sinks are thermal black body radiation at the surface and heat conduction into the volume of the wall. On the inner wall, convective cooling caused by the liquid fuel will appear as an additional heat sink, as long as the irradiated part of the tank is fueled.

This heat transfer problem cannot be solved analytically, as the incoming laser intensity varies with time and the material parameters of the wall are temperature dependent. For that reason a numerical model was implemented, using the commercial software COMSOL Multiphysics. COMSOL uses the Finite Element Method (FEM) to solve the heat transfer equation. Details about the application of the FEM to solve those problems can be found in the literature.[90]

To validate the devised model, a number of experiments have been undertaken during one of the authors dissertation work.[91] One experimental setup is illustrated in Figure 19. A sheet metal is irradiated with a laser beam and

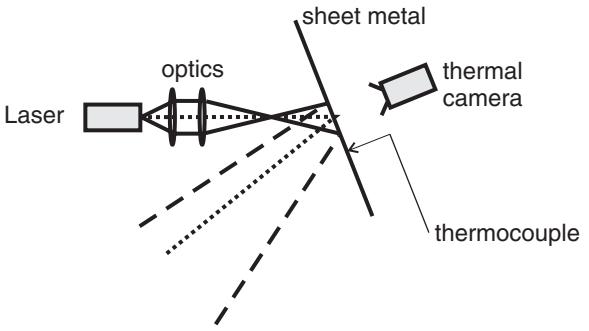

Figure 19: Experimental setup for temperature measurements of sheet metals. A sheet of metal is radiated with a laser beam. The temperature increase at the specimen's backside is measured by a thermal camera, which is shielded from beam exposure by the specimen. An additional thermocouple is used to verify the measurement.

the resulting temperature distribution is measured with a thermal camera from the back side of the specimen. A continuous laser with a wavelength of 1,03 μm is used, the maximum output power is 1270 W. Beam diameter and output power are varied for different experiments, translating to intensities between 100 W/cm^2 and 3200 W/cm^2. Aluminium and steel sheets with a thickness of one to two millimeters are used as specimens. The thickness of the sheets as well as the laser intensities match the parameters of the chosen missile defense scenario. Figure 20 shows the comparison of model predictions and experimental results for one example, please refer to the caption for details. The temperatures predicted by the model are in good agreement with the measurement.[92]

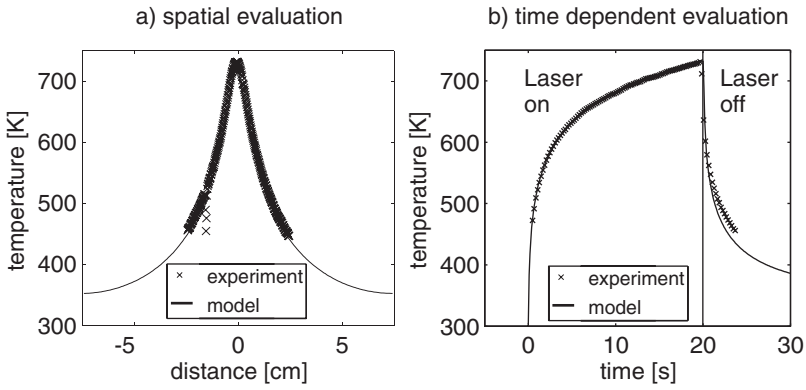

Figure 20: Validation of model predictions with experimental results. Specimen: Al99, 2 mm thickness. Laser: wavelength $\lambda = 1.03$ μm, beam radius on target 0.5 cm, laser power 1270 W (continuous) *Left:* temperature distribution on a line crossing the center of the beam after 20 s irradiation. At approximately -1 cm, the camera's field of view is blocked by a thermocouple (see Figure 19). *Right:* maximum temperature over time, including a time where the laser is turned off.

Temperature Calculations for the Presented Case Study

The devised numerical model is used to calculate the temperature distribution in the wall of a tank section of the missile during the course of a missile defense engagement. Table 3 summarizes the input parameters for the model. The aluminium alloy AL 5083 is chosen because it has been used for liquid propellant missiles in the past.[93] Details about the temperature dependent thermo-physical properties of this material can be found in Appendix D. The chosen wall width is the lower boundary of values published by UNMOVIC and Forden,[94] the diameter matches values published by Wright.[95]

The model is restricted to a cylinder with a height of 2/3 the missile's diameter. This height is used, because it is the commonly used distance between two reinforcing rings, which are used to stabilize the tank. The upper and lower boundaries are assumed to be thermally insulated. That way it is guaranteed that the temperature is not underestimated in case the beam diameter is extending the modeled section. The wall is assumed to be thin, resulting in a uniform temperature throughout d. The resulting error of this assumption is negligible, as conducted fully three dimensional calculations show.

The heat flux at the outer boundaries is assessed as follows:

- Heat flux caused by the *incoming laser intensity* according to Eq. 3 is determined by the absorption A of the missile's surface. Although in general, A is temperature dependent, for the assessed temperature range it is approximately a constant.[96] In theory, A can range between zero and one. The absorption could be near one for a highly absorbing surface. For multilayer dielectric coatings the value could be near zero. A gold coating would have an absorption of 0.01 at the ABL's wavelength.[97] The absorption of an aluminium surface at the ABL's wavelength can range between 0.30 and 0.04, depending on surface quality and oxidation, with 0.04 representing a highly polished surface.[98] For this research, a value of 0.10 is chosen, because this also represents the absorption of a simple white paint.[99] In the presence of an ABL, a state launching a missile would probably take at

Table 3: Input parameters for the temperature calculations

Wall material	AL 5083-H321
Wall width	2 mm
Diameter	1.3 m
Coating	white paint
Absorption (at $\lambda = 1.315\ \mu$m)	0.1
Emissivity	0.9
Initial temperature	293 K

least the measure of using white paint in order to increase the probability of a successful flight. If the ABL is fielded, gold coatings could not be ruled out in the long run, but at this point a white paint seems to be more likely. A 0.10 absorption results in a maximum heat flux of 30 W/cm^2 for the presented case.

- Heat losses by black-body *thermal radiation* are taken into account using the Stefan-Boltzmann law. An emissivity of 0.9 is assumed, which conforms to white paint.[100]

- *Convective heat flux* occurs on the outside as well as the inside of the tank section. On the outside, aerodynamic heating will occur as soon as the missile is accelerated to a velocity faster than the speed of sound.[101] Depending on the aerodynamics of the problem, this can result in a heat flux between 3 W/cm^2 and 20 W/cm^2 for a turbulent boundary layer, or approximately half of that for a laminar flow.[102]
  The most significant factor on the inside is cooling caused by the liquid fuel. If the fuel near the missile wall reaches its boiling point, it acts like a heat sink with heat fluxes up to 400 W/cm^2.[103] The boiling points for common missile fuels are well beyond significant temperature increases.
  Both convective effects are therefore significant for an ABL engagement. While cooling by liquid fuel would prevent any significant heating, heating could give the laser a head start. In reality, the interplay between both effects can determine the outcome of an ABL engagement. As long as the irradiated location of the tank section is still filled by liquid fuel, no significant temperature increase will occur for the examined single-walled missiles. After the tank is emptied out, aerodynamic heating might be significant, but this strongly depends on the position of the aim point on the missile. For example, on the tip of the Ariane 1, a temperature increase of about 150 K occurs during its boost phase, while on the lower edge of the payload's shroud only an increase of 10 K was measured.[104]
  At this point, both cooling and heating by convection are neglected. The possible effects of this assumption on the results of this case study are tested later.

These assumptions define the heat flux, resulting in the following equation defining the boundary condition for the heat equation:

$$q(\vec{r},t)\big|_{\vec{r}\in\text{surface}} = -\vec{\text{N}}_{\text{surf}} \cdot (\kappa\ \text{grad}(T)) = AI_{\text{eff}} - \epsilon\sigma\left(T^4 - T_{\text{U}}^4\right). \tag{17}$$

Using the intensity $I(x,y,z,t)$ calculated in the last section and an initial temperature of 293 K, the temperature distribution is calculated. Figure 21 illustrates the temperature distribution after 68 s flight time for the case of maximum anisoplanatism. Figure 22 shows the maximum temperature during the

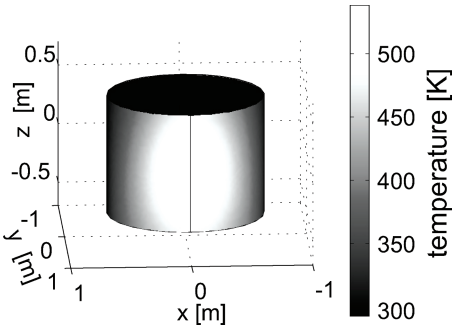

Figure 21: Calculated temperature for the examined case study (compare to Figure 3). Shown is the temperature distribution after 68 s flight time for an intensity distribution according to the case of full anisoplanatism.

flight time for the cases of full anisoplanatism and reduced anisoplanatism. For both cases, the maximum temperature during the boost phase does not exceed the melting temperature of aluminium, which is approximately 930 K. For this reason, a more sophisticated damage assessment is undertaken, including the effects of mechanical stress.

APPENDIX C: CALCULATING MECHANICAL STRESS

Introduction

Materials can only sustain a certain amount of mechanical stress σ. Stress is defined as force F per area A. Figure 23 a) illustrates the behavior for a

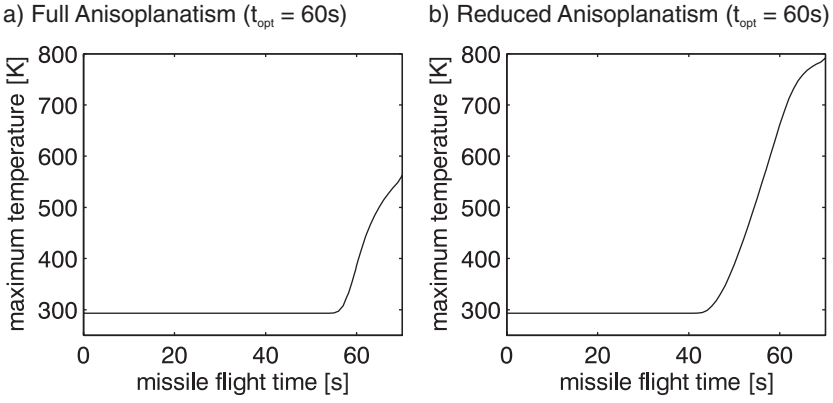

Figure 22: Calculated temperature for the examined case study (compare to Figure 3). Shown is the maximum temperature for two cases of different incoming intensity during the boost phase.

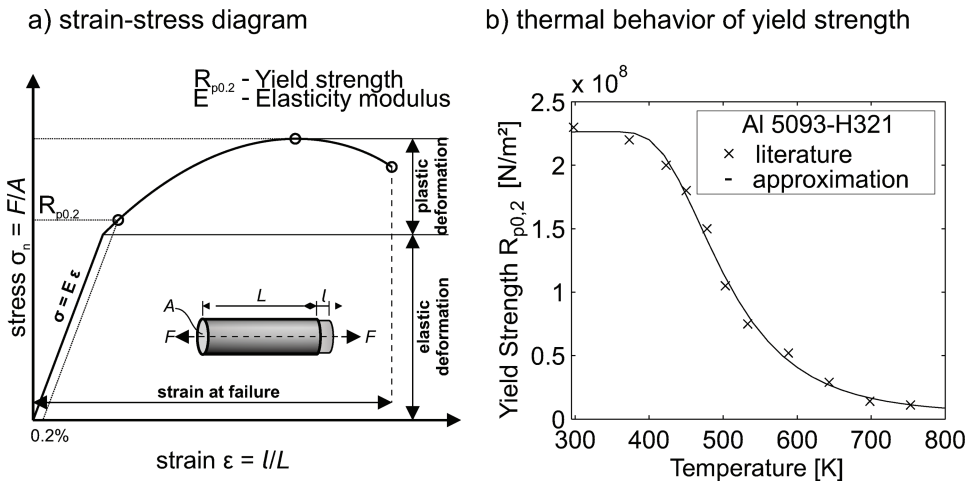

Figure 23: Definition and temperature behavior of yield strength $R_{p0.2}$. a) As the mechanical stress exceeds the yield strength, plastic deformation occurs. A further increase leads to strong deformation and finally failure of the material. b) Yield strength is temperature dependent. Sources: a) adapted from Sigmund[105] b) Data points: Kaufman[106]

ductile metal alloy. Increasing stress σ leads to elongation of a specimen. The relative elongation is called strain ε. In the elastic regime, the elongation is reversible. If the force disappears, the specimen will return to its original shape. In the case of plastic deformation, some elongation will sustain. If this sustained deformation exceeds 0.2 percent, per definition, the stress has exceeded the yield stress $R_{\mathrm{p0.2}}$, which is also called the yield strength or the elastic limit. If the stress is increased above this limit, extensive deformations will occur. Further increasing stress will finally lead to a failure of the material. As deformation interferes with the operation of a structure, $R_{\mathrm{p0.2}}$ is decisive to assess to implications of mechanical stress.

For the case of laser missile defense it is important to notice that $R_{\mathrm{p0.2}}$ is strongly dependent on temperature. The aluminium alloy Al 5083, chosen for our case study, loses about 80 percent in yield strength, if its temperature is raised 300 K from room temperature, as illustrated in Figure 23 b). An ABL missile defense engagement leads to rising temperatures in the wall, which will lower the value of $R_{\mathrm{p0.2}}$. As soon as $R_{\mathrm{p0.2}}$ is diminished to the stress level inside the wall, plastic deformation starts to occur. This does not imply instantaneous material failure and destruction of the missile, but gives the lower boundary for significant effects of laser heating. For the scope of this study, $R_{\mathrm{p0.2}}$ is chosen as indication for a successful missile defense engagement. This can be understood as a best-case analysis in favor of the ABL.

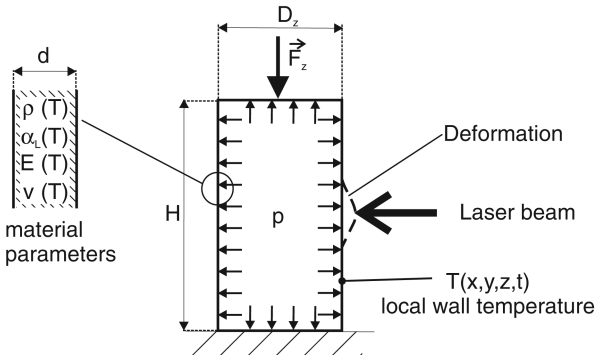

Figure 24: Problem setup for stress calculations for a missile body. A schematic cutaway of a fuel tank and the driving forces and loads during a missile defense engagement are shown. The tank is internally pressurized (p), external forces are approximated by an axial load $\vec{F}_z$. The material parameters are temperature dependent, hence they are influenced by the laser-induced temperature field.

Assessment Method

Figure 24 illustrates the problem setup for the stress assessment of the irradiation of a missile's tank section. The pressure inside the tank is kept constant by an external pressure supply, as this stabilizes the thin walled cylinder and helps fuel the turbo-pumps for the engine.[107] During the acceleration, the missile's engine provides a force $\vec{F}_z$ approximately parallel to the axis of the cylinder. According to Newton's third law, this force is equal to the sum of gravity, inertia and drag forces at the lowest point of the missile. In order to evaluate maximum stress, this maximum force is applied for the calculations of the case study.

The laser beam induces the calculated time-dependent temperature field. An increased temperature implies a thermal expansion of the material and a change in the material parameters. These parameters are the density ϱ, the thermal expansion coefficient α_L, Young's modulus of Elasticity E and Poisson's ratio ν. All these parameters are temperature dependent. Further input parameters are the thickness of the wall d, the diameter of the tank section D_z and its height H.

The choice of $R_{p0.2}$ as assessment parameter restricts our mechanical calculations to the elastic regime. Hooke's law is valid in good approximation and the relationship between stress and strain is linear:

$$\sigma = E\varepsilon. \tag{18}$$

The given problem is a three-dimensional setup. Instead of a linear elongation, it involves arbitrary deformation of a solid body as the result of external forces. In continuum mechanics, this deformation is described using displacement

vectors. The new location of a certain element of the solid after its displacement is indicated by a displacement vector $\vec{U}(x, y, z, t)$, or using the displacement coordinates u, v and w.

$$\vec{U}(x, y, z, t) = \begin{pmatrix} u(x, y, z, t) \\ v(x, y, z, t) \\ w(x, y, z, t) \end{pmatrix}. \tag{19}$$

Stress, strain, as well as Young's modulus are described using tensors. For example, in general strain is given by the tensor $\hat{\varepsilon}$:

$$\hat{\epsilon} = \begin{bmatrix} \epsilon_{xx} & \epsilon_{xy} & \epsilon_{xz} \\ \epsilon_{yx} & \epsilon_{yy} & \epsilon_{yz} \\ \epsilon_{zx} & \epsilon_{zy} & \epsilon_{zz} \end{bmatrix} \quad \text{where} \quad \begin{aligned} \epsilon_{xx} &= \frac{\partial u}{\partial x} \\ \epsilon_{yy} &= \frac{\partial v}{\partial y} \\ \epsilon_{zz} &= \frac{\partial w}{\partial z} \end{aligned} \quad \text{and} \quad \begin{aligned} \epsilon_{xy} &= \frac{1}{2}\left(\frac{\partial u}{\partial y} + \frac{\partial v}{\partial x}\right) \\ \epsilon_{yz} &= \frac{1}{2}\left(\frac{\partial v}{\partial z} + \frac{\partial w}{\partial y}\right) \\ \epsilon_{xz} &= \frac{1}{2}\left(\frac{\partial u}{\partial z} + \frac{\partial w}{\partial x}\right) \end{aligned}. \tag{20}$$

Similar definitions apply for the stress tensor and the material parameters, as described in the literature on continuum mechanics. The stress tensor is evaluated using principal component analysis. The resulting first principle stress is the largest occurring stress, which is compared to the yield strength of the material.

Hooke's law is also adaptable to three dimensions. If thermal expansion is added, it is given by:

$$\hat{\sigma} = \hat{E} \cdot (\hat{\epsilon} - \hat{\epsilon}_{\text{therm}}) \qquad \text{while} \quad \hat{\epsilon}_{\text{therm}} = \hat{\alpha}(T - T_0). \tag{21}$$

where T_0 is the initial temperature and T is the Temperature field at a time t.

Equation 21 describes the material behavior in the wall. To solve the entire mechanical problem, internal and external forces have to be balanced. As for the thermal model, a numerical approach is chosen, using the finite element software COMSOL.

The implemented numerical model used for temperature calculations is extended to calculate mechanical stresses. The time-dependent temperature field is the driving factor for the mechanical model, resulting in thermal expansion and changing material parameters. For each time, the temperature dependent $R_{p0.2}(T)$ is locally compared to the occurring stresses in order to find out the missile flight times required for the laser to inflict significant damage.

The model has been successfully validated in scaled experiments during one of the author's dissertation work.[108] Please refer to the acknowledgements of this paper for a list of involved institutions. Small (163 mm height) pressurized hollow cylinders[109] have been irradiated and the time dependent deformation was measured during the irradiation process using a pattern projection method developed by Bothe et al.[110] The change in cylinder radius is

a) experimental setup

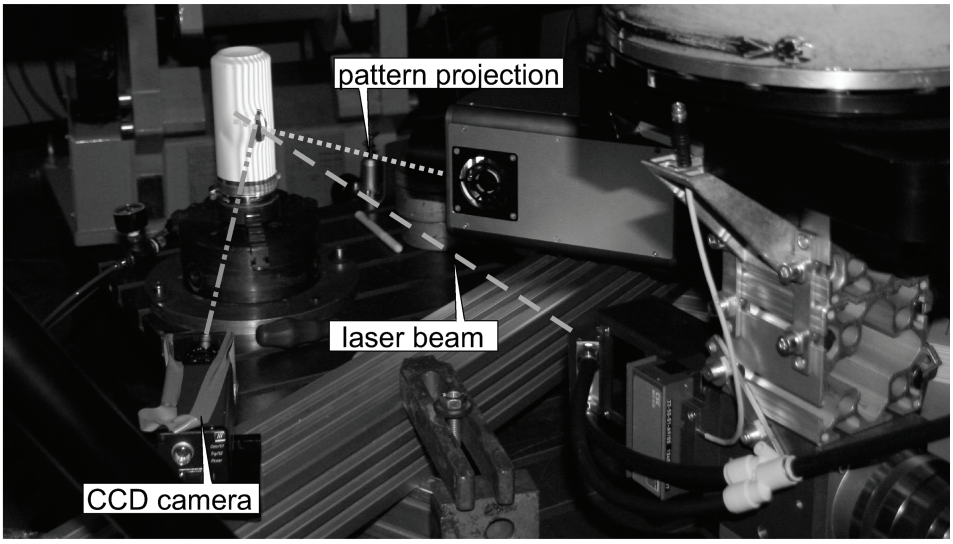

b) measurement of deformed cylinder radius

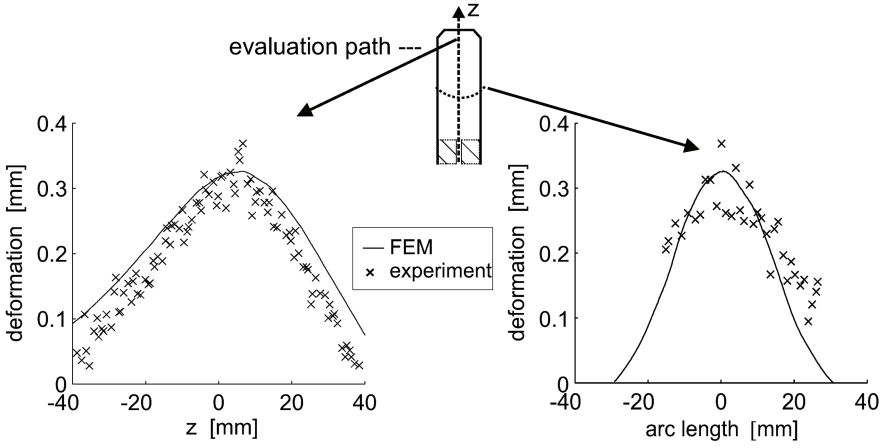

evaluation along axial coordinate z

evaluation along cylinder circumference

Figure 25: Experimental validation of mechanical model. The deformation of the cylinder is measured during laser irradiation. Specimen: Hollow cylinder with 66 mm diameter, 163 mm height, wall thickness 0.1 mm, material Al 3104, coated with white paint (TiO_2), internal pressure 1.5 bar; Laser: power=200 W (continuous), beam radius on target 3 cm, 40 s irradiation time, the measurement took place at 40 s during irradiation.

compared to the model predictions. The experimental setup and one illustrative measurement are shown in Figure 25.

In addition to deformation measurements, sample failure tests with the same specimens have been conducted. In those cases, irradiation of the

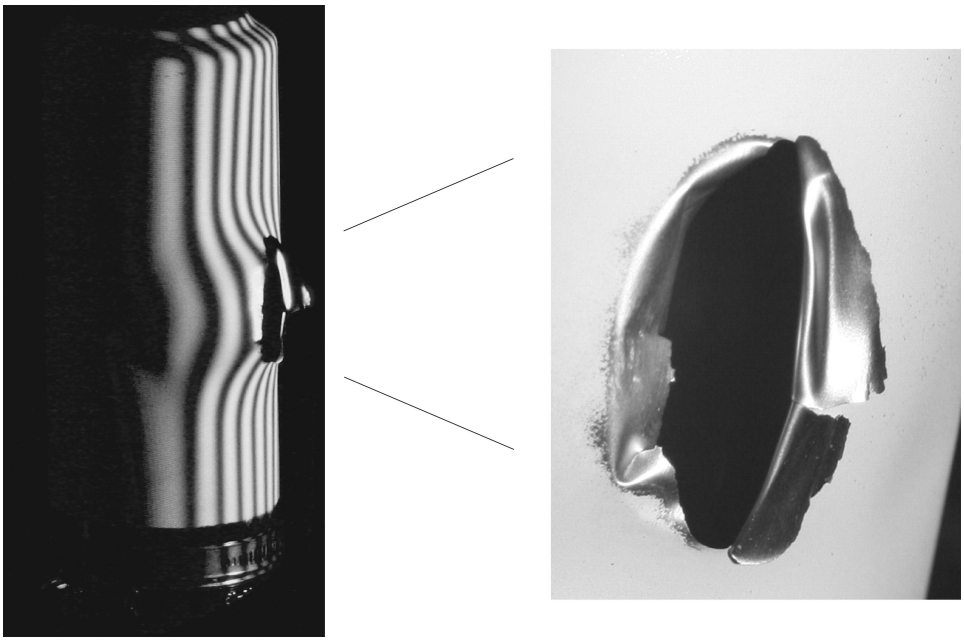

Figure 26: Laser irradiation of a hollow cylinder until material failure. Failure occurred after 4.5 s at approximately 600 K at the temperature maximum. Setup: internal cylinder pressure: 2 bar, beam diameter 7.5 cm, laser power 1 kW, cylinder data as in Figure 25.

samples was conducted until material failure. For the case illustrated in Figure 26, material failure occurred about 300 K below the melting point. The residual plastic deformation is clearly noticeable. This is consistent with the model, which for this case predicts that mechanical stress exceeding the elastic limit after 2.7 s, while failure was observed after 4.5 s.

Stress Calculations for the Presented Case Study

As the mechanical model is an extension of the thermal model, it is using the same geometric parameters compiled in Table 3. Additional mechanical parameters can be found in Table 4. The behavior of a tank section between two reinforcing rings is assessed. It is assumed that the wall material is welded onto these reinforcing rings, as is common for liquid fuel missiles.[111]

Table 4: Input parameters for stress calculation

Internal pressure	2 bar
Thrust	$5{\cdot}10^5$ N
Geometry	see table 3
Temperature field	as calculated before

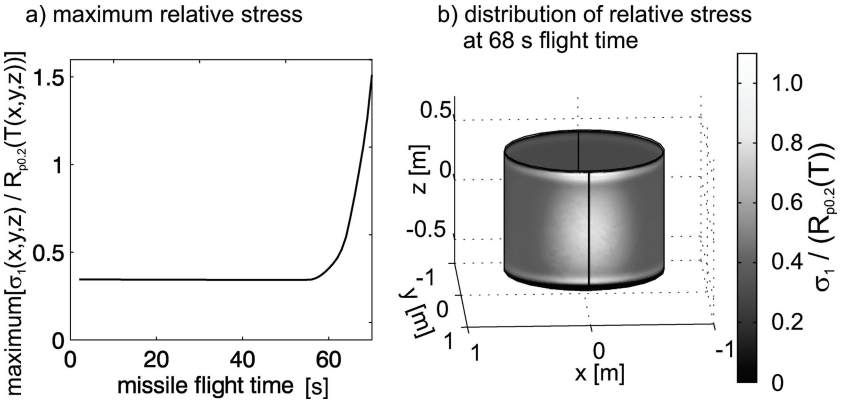

Figure 27: Stress calculation for the examined case study (compare to Figure 3). Relative stress for the case of full anisoplanatism; a) Maximum relative stress during the boost phase b) stress distribution in the cylinder at 68 s flight time.

As boundary conditions, one ring is fixed in space, while the other is under a constant load by the engine's thrust, parallel to the axis of the undeformed cylinder. This translates into a compressive load for the cylinder. In addition, there is a constant load on the cylinder walls as the result of internal pressure. The assumed thrust is chosen in accordance to the analysis of the Nodong missile by Wright and Kadyshev.[112] The internal pressure for liquid propellant missile commonly ranges between 1 bar and 2 bar.[113] In order to allow for a best case analysis in favor of the ABL, the upper limit is chosen.

Figure 27 shows the distribution of relative stresses along the cylinder wall after 68 s flight time, for an intensity distribution according to full anisoplanatism. If the relative stress exceeds unity at a certain location, the first principle stress exceeds the temperature dependent elastic limit at that point. In the case of full anisoplanatism this does occur after 68 s of flight time. At this point, the mechanical stress exceeds the elastic limit near the reinforcing rings and at the temperature maximum. This happens at those locations, as the maximum temperature introduces the maximum reduction of tensile strength and deformation is restricted at the location of the reinforcing rings, leading to extended mechanical stress at that point.

For the case of reduced anisoplanatism (Figure 15 d)), relative stresses exceed the elastic limit much earlier. An optimization of the aim point (according to minimal anisoplanatism at $t_{\mathrm{opt}} = 45\ s$) leads to critical stresses after 47 s of missile flight time.

APPENDIX D: EMPLOYED PARAMETERS FOR THE ASSESSED SCENARIOS

Trajectory Parameters for the Mid-Range Missile Defense Case Study

Model parameters are based on an analysis by Wright and Kadyshev.[114] The trajectory was calculated using GUI_Missile_Flyout Version 2.02 by G. E. Forden.[115]

Table 5: Missile parameter

Parameter	Value	
Specific impulse	240	s
Burn time	70	s
Propellant mass	16000	kg
Empty weight	3900	kg
Payload	1000	kg
Thrust	$5{\cdot}10^5$	N

Table 6: Launch parameter

Parameter	Value	
Latitude	41.064	° North
Longitude	126.784	° East
Altitude	0	m
Azimuth	160.9732	°
Loft angle	45.032	°
Loft angle rate	6.522	°/s

Clear-1 Night Parametric Turbulence Model

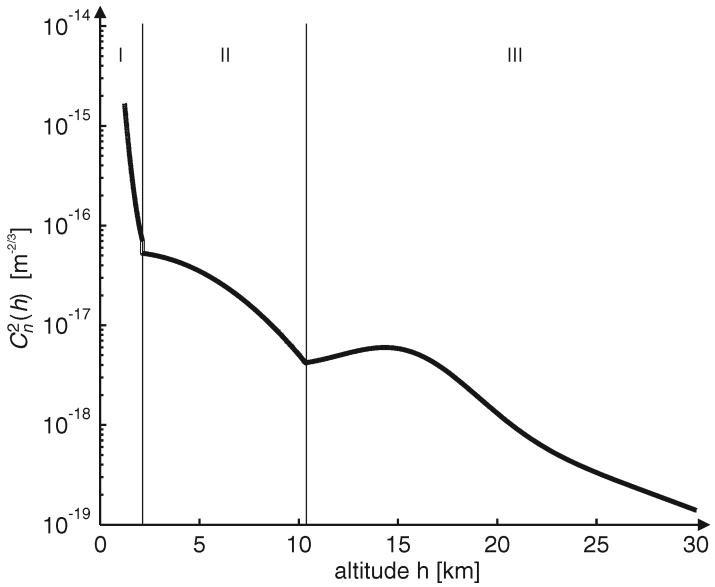

I: 1.23 km $< h \leq$ 2.13 km

$\log_{10}(C_n^2(h)) = A + Bh + Ch^2$

$A = -10.7025 \quad B = -4.3507 \quad C = +8.1414$

II: 2.13 km $< h \leq$ 10.34 km

$\log_{10}(C_n^2(h)) = A + Bh + Ch^2$

$A = -16.2897 \quad B = +0.0335 \quad C = -0.0134$

III: 10.34 km $< h \leq$ 30 km

$\log_{10}(C_n^2(h)) = A + Bh + Ch^2 + De^{-0.5((h-E)/F)^2}$

$A = -17.0577 \quad B = -0.0449 \quad C = -0.0005$

$D = +0.6181 \quad E = +15.5617 \quad F = +3.4666$

Figure 28: Dependence of turbulence on altitude according to the turbulence model CLEAR 1 night, adapted from Beland.[116]

Employed Parameters to Assess Target Interaction

Table 7: Employed thermo-physical parameters.

Parameter		Approximation (T (K))	Source
Thermal conductivity κ	W/m K	$3.182847 \cdot 10^{-7} \cdot T^3$ $-6.570887 \cdot 10^{-4} \cdot T^2$ $+0.4662148 \cdot T + 30.01698$	117a
Heat Capacity c_p	J/kg K	955.32	118a
density ρ	kg/m^3	$1.007566 \cdot 10^{-12} \cdot T^5$ $-2.270152 \cdot 10^{-9} \cdot T^4$ $+2.004492 \cdot 10^{-6} \cdot T^3$ $-9.256705 \cdot 10^{-4} \cdot T^2$ $+0.03368339 \cdot T + 2699.543$	119a
Emissivity ε[b]		0.9	120
Absorptance A		0.1	c

[a]the cited source provided the approximation function.
[b]according to finishing on the inside and the outside.
[c]according to white paint or mid-qualtity aluminium surface at a wavelength $\lambda = 1.315\ \mu$m.

Table 8: Employed thermo-structural parameters for AL5083-H321.

Parameter		Approximation (T (K))	Source
Youngs's modulus E	N/m^2	$-14673.07 \cdot T^2 - 3.192493 \cdot 10^7 \cdot T$ $+8.239008 \cdot 10^{10}$	121
thermal exp. coeff. α_L	1/K	$1.742129 \cdot 10^{-14} \cdot T^3$ $-3.563214 \cdot 10^{-11} \cdot T^2$ $+3.06124 \cdot 10^{-8} \cdot T + 1.640353 \cdot 10^{-5}$	122
Poisson-ratio ν		0.334	123
$R_{p0.2}$	N/m^2	$b - (b - a) \cdot \exp(-c \cdot (T^d))$ where $a = 3.74 \cdot 10^6$; $b = 2.26 \cdot 10^8$; $c = 4.56 \cdot 10^{19}$; $d = -7.34$	124a

[a]valid 245 K to 813 K, approximation according to data points provided by Kaufman.

Table 9: Employed parameters for additional case studies.

	Short range missile	Satellite
Diameter	0.88	4.2 m
Material	steel S30200	aluminium AL7075
Thickness	3 mm	1.2 mm
Internal pressure	5 bar	—
Thrust	170000 N	—
Burn time	75 s	—

NOTES AND REFERENCES

1. T. H. Maiman, "Optical and Microwave-Optical Experiments in Ruby," *Phys. Rev. Lett.* 4, no. 11 (June 1960): 564–566, doi:10.1103/PhysRevLett.4.564.

2. National Museum of the United States Air Force, ed., *Texas Instruments BOLT-117 Laser Guided Bomb* (2002), http://www.nationalmuseum.af.mil/factsheets/factsheet.asp?id=1014 (accessed Mar. 15, 2009); *M1 Abrams Main Battle Tank* (2004), http://www.globalsecurity.org/military/systems/ground/m1-intro.htm (accessed Mar. 30, 2009).

3. J. H. McCall Jr., "Blinded by the Light: International Law and the Legality of Anti-Optic Laser Weapons," *Cornell International Law Journal* 30, no. 1 (1997): 1–44.

4. W. M. Arkin and A. Peters, "U.S. Blinding Laser Weapons," *Human Rights Watch Arms Project* 7. no. 5A (May 1995), http://www.hrw.org/reports/1995/Us2.htm (accessed Mar. 30, 2009).

5. L. Doswald-Beck, "New Protocol on Blinding Laser Weapons", *International Review of the Red Cross* 312 (1996): 272–299.

6. Bill Gertz, "Revealed: N. Korea Fired Laser at U.S. troops," *The Washington Times* (May 13, 2003): A01, http: //www. gertzfile.com/gertzfile/article5.13.03.html (accessed Sept. 30, 2009).

7. Doug Beason, *The E-bomb: How America's New Directed Energy Weapons Will Change the Way Future Wars Will Be Fought* (Da Capo Press, 2005), p. xii, ISBN: B000VY9B1Y.

8. Clarence A. Robinson Jr., "Beam Weapons Technology Expanding," *Aviation Week & Space Technology,* May 25, 1981, 40.

9. G. Forden, "Ballistic Missile Defense: The Airborne Laser," *IEEE Spectrum* 34, no. 9 (Sept. 1997): 40–49; Geoffrey E. Forden, *Shooting Down What's Going Up,* Working Paper (Stanford University, Stanford, CA: Center for International Security and Arms Control, Sept. 1997), http://iis-db.stanford.edu/pubs/10326/forden.pdf (accessed Mar. 27, 2009).

10. D. K. Barton et al., "Report of the American Physical Society Study Group on Boost-Phase Intercept Systems for National Missile Defense: Scientific and Technical Issues," *Reviews of Modern Physics* 76, no. 3 (2004): S1–S424.

11. Mordechai Rokni and Allen Flusberg, "Stimulated Rotational Raman Scattering in the Atmosphere," *Quantum Electronics, IEEE Journal of* 22, no. 7 (July 1986): 1102–1108.

12. J. Stupl and G. Neuneck, "High Energy Lasers: A Sensible Choice for Future Weapons Systems?" *Security Challenges* 1, no. 1 (Nov. 2005): 135–153, http://www.securitychallenges.org.au/ArticlePDFs/vol1no1StuplandNeuneck.pdf.

13. Boeing, *Boeing Conducts Successful Avenger-Mounted Laser Tests—Innovative System Neutralizes lEDs, Unexploded Ordnance* (St. Louis: press release, 2007), http://www.boeing.com/news/releases/2007/q4/071015a_nr.html (accessed Mar. 27, 2009); Boeing, *Boeing Laser Avenger Shoots Down Unmanned Aerial Vehicle in Tests,* January 26 (St. Louis: press release, 2009), http://www.boeing.com/news/releases/2009/q1/090126a_nr.html (accessed Mar. 27, 2009).

14. Boeing, *Boeing Laser Avenger Shoots Down Unmanned Aerial Vehicle in Tests.*

15. Atmospheric particles scatter a small fraction of the laser beam in all directions.

16. Boeing, *Boeing Fires New Thin-Disk Laser, Achieving Solid-State Laser Milestone* (St. Louis: press release, 2008), http://www.boeing.com/news/releases/2008/q2/

080603a_nr.html (accessed Sept. 27, 2009); Boeing, *Boeing Laser System Redeploys Quickly, Then Tracks Targets and Fires Laser* (press release, 2009), http: //www.boeing.com/news/releases/2009/q1/090324a_nr.html (accessed Mar. 27, 2009); Lynn Farrow, "Out of the Future—A Team Works on a System that will Demonstrate Laser Weapons' Capabilities," *Boeing Frontiers* (Mar. 2009), http://www.boeing.com/news/frontiers/archive/2009/march/i_ids05.pdf (accessed Mar. 27, 2009).

17. Raytheon Company Missile Systems, *Laser Area Defense System—Close-in Protection Against Asymmetric Threats* (Tucson, Arizona: press release, 2007), http://www.raytheon.com/newsroom/feature/stellent/groups/public/documents/content/cms04_025223.pdf (accessed Mar. 27, 2009); Mike Booen, *Raytheon's Directed Energy Solutions—Transitioning DEW to the Warfighter (Finally),* presentation slides (2008), http://airdefenseartillery.com/ada_website_08/attach/C-RAM.pdf (accessed Mar. 27, 2009); Drew Hamilton, *White Sands Testing New Laser Weapon System,* Official Homepage of the U.S. Army/News Front Page (2009), http: //www.army.mil/-news/2009/01/30/16279-white-sands-testing-new-laser-weapon-system/ (accessed Mar. 27, 2009).

18. Northrop Grumman, *Northrop Grumman Scales New Heights in Electric Laser Power, Achieves 100 Kilowatts From a Solid-State Laser* (Redondo Beach, CA: press release, 2009), http://www.irconnect.com/noc/press/pages/news_releases.html?d=161575 (accessed Mar. 27, 2009).

19. Doug Beason, *The E-bomb: How America's New Directed Energy Weapons Will Change the Way Future Wars Will Be Fought* (Cambridge, Mass.: Da Capo Press, 2005).

20. U.S. Department of Defense, *Fiscal Year (FY) 2008/FY 2009 Budget Estimates Office of the Secretary of Defense (OSD) RDT&E Descriptive Summaries, Volume 3, 0603750D8Z—Advanced Concept Technology Demonstrations (P523)* (2007), 122, http://www.defenselink.mil/comptroller/defbudget/fy2008/budget_justification/pdfs/rdtande/Vol_3_OSD/BA-3.pdf (accessed Nov. 23, 2007); Walter Poll, "Fielding Laser Dreams", *Boeing Frontiers* (June 2007): 26–27, http://www.boeing.com/news/frontiers/archive/2007/june/i_ids04.pdf (accessed Aug. 24, 2009).

21. John Pike, *Advanced Tactical Laser (ATL)* (2005), http://www.globalsecurity.org/military/systems/aircraft/systems/atl.htm (accessed July 1, 2009).

22. Bill Sweetman, "Fact or Fiction—Briefing Directed Energy Lasers," *Jane's Defense Weekly,* Feb. 22, 2006, 25–29; George Fenton, "The U.S. Department of Defense Joint Non-Lethal Weapons Program," in *National Defense Industrial Association (NDIA) Non-Lethal Defense IV, 20–22 March 2000, Tysons Corner, VA,* information in backup slides (p. 26–27) (2000), http://web.archive.org/web/20011109023659/www.dtic.mil/ndia/nld4/fenton.pdf (accessed May 20, 2009)

23. Fenton, "The U.S. Department of Defense Joint Non-Lethal Weapons Program."

24. Boeing, *Boeing Awarded Contract to Continue Testing Advanced Tactical Laser* (press release, 2008), http://boeing.mediaroom.com/index.php?s=43&item=434 (accessed June 5, 2009).

25. Boeing, *Boeing Advanced Tactical Laser Fires High-Power Laser in Flight* (press release, 2009), http://boeing.mediaroom.com/index.php?s=43&item=703 (accessed June 16, 2009).

26. More information about boost-phase missile defense can be found at D. K. Barton et al., "Report of the American Physical Society Study Group on Boost-Phase Intercept Systems for National Missile Defense: Scientific and Technical Issues," *Reviews of Modern Physics* 76, no. 3 (2004): S1–S424.

27. Barton et al., "Report of the American Physical Society Study Group on Boost-Phase Intercept Systems for National Missile Defense: Scientific and Technical Issues"; Forden, "Ballistic Missile Defense: The Airborne Laser."

28. Christopher Bolkcom and Steven A. Hildreth, *Airborne Laser (ABL): Issues for Congress,* CRS Report for Congress, RL32123, technical report (July 9, 2007), http://fas.org/sgp/crs/weapons/RL32123.pdf (accessed Mar. 30, 2009).

29. Bolkcom and Hildreth, *Airborne Laser (ABL): Issues for Congress;* U.S. Department of Defense—Office of the Under Secretary of Defense (Comptroller), *Department of Defense Fiscal Year (FY) 2010 Budget Estimates—Research, Development, Test, and Evaluation—Volume 2: Missile Defense Agency (MDA)—MDA Exhibit R-2 — PE 0603883C* (2009), http://www.defenselink.mil/comptroller/defbudget/fy2010/budget_justification/pdfs/03-RDT_and-E/VoL2_MDA/PE-0603883C-Boost-Defense.pdf (accessed May 28, 2009).

30. U.S. Department of the Air Force, *Supporting Data for Fiscal Year 1999 Amended Budget Estimates—Research, Development, Test and Evaluation—Descriptive Summaries—Volumes I, II, & III—RDT&E Budget Item Justification Sheet (R-2 Exhibit)—0603319F Airborne Laser Program—Project 4269* (1998), http://www.saffm.hq.af.mil/shared/media/document/AFD-070223-247.pdf (accessed Apr. 15, 2009).

31. InsideDefense.com, *ABL Shoot-Down Test Rescheduled for December-February Time Frame* (2009), http://defense.iwpnewsstand.com/showdoc.asp?docnum=AIRFORCE-20-44-19 (accessed Nov. 9, 2009).

32. House Armed Services Committee United States House of Representatives, *Unclassified Statement of Lieutenant General Patrick J. O'Reilly, Director, Missile Defense Agency before the House Armed Services Committee Subcommittee on Strategic Forces regarding the Fiscal Year 2010 Missile Defense Programs, Thursday, May 21, 2009* (2009), http://armedservices. house. gov/pdfs/SF052109/OReilly_Testimony052109.pdf (accessed May 28, 2009).

33. Boeing, *Boeing Airborne Laser Team Begins Weapon System Flight Tests* (press release, 2009), http://www.boeing.com/news/releases/2009/q2/090424a_nr.html (accessed Apr. 27, 2009); Missile Defense Agency, *Airborne Laser Begins Final Proof-of-Concept Tests* (press release, 2009), http://www.mda.mil/mdaLink/pdf/09news0009.pdf (accessed Apr. 27, 2009).

34. U.S. Department of Defense, *DoD News Briefing With Secretary Gates From The Pentagon—4 April 2009* (2009), http://www.defenselink.mil/transcripts/transcript.aspx?transcriptid=4396 (accessed Apr. 27, 2009).

35. House Armed Services Committee United States House of Representatives, *Unclassified Statement of Lieutenant General Patrick J. O'Reilly, Director, Missile Defense Agency before the House Armed Services Committee Subcommittee on Strategic Forces regarding the Fiscal Year 2010 Missile Defense Programs, Thursday, May 21, 2009;* Reuters, *BRIEF—Pentagon to decide fate of Boeing laser in 2010* (2009), http://uk.biz.yahoo.com/07052009/323/brief-pentagon-decide-fate-boeing-laser-2010.html (accessed May 28, 2009); Amy Butler, "ABL Laser Gets MDA Nod Thus Far," *Aerospace Daily and Defense Report,* June 3, 2009, http://www.aviationweek.com/aw/generic/story_channel.jsp?channel=defense&id=news/ABL060309.xml (accessed June 9, 2009).

36. Bolkcom and Hildreth, *Airborne Laser (ABL): Issues for Congress.*

37. Jan Stupl, *Untersuchung der Wechselwirkung von Laserstrahlung mil Strukturelementen von Raumflugkörpern* (Verlag Dr. Hut, 2008), http://www.sub.uni-hamburg.de/opus/volltexte/2008/3951/.

38. Barton et al., "Report of the American Physical Society Study Group on Boost-Phase Intercept Systems for National Missile Defense: Scientific and Technical Issues," p. xxii, 318.

39. David C. Wright and Timur Kadyshev, "An Analysis of the North Korean Nodong Missile," *Science & Global Security* 4, no. 2 (1994): 129–160, http://www.princeton.edu/~globsec/publications/pdf/4_2wright.pdf.

40. U.S. Defense Intelligence Agency, *North Korea: The Foundations for Military Strength—Update 1995,* PC-1510-101-96, technical report (Washington, DC, Dec. 1995), http://fas.org/irp/dia/product/knfms95/1510-101_toc.html (accessed Sept. 19, 2008); Chung-In Moon, "Changing Threat Environment, Force Structure, and Defense Planning: the South Korean Case," in *Emerging Threats, Force Structures and the Role of Air Power in Korea* (Santa Monica, CA: RAND, 2000), 89–114, http://www.rand.org/pubs/conf_proceedings/2007/CF152.pdf (accessed Sept. 19, 2008).

41. Geoffrey Forden, "GUI_Missile_Flyout: A General Program for Simulating Ballistic Missiles," *Science & Global Security* 15, no. 2 (2007): 133–146, http://www.princeton.edu/~globsec/publications/SciGloSec.shtml.

42. Forden, *Shooting Down What's Going Up,* p. 11–13.

43. To calculate the remaining trajectory with increased drag, GUI_Missile_Flyout is used. At 47s, the diameter of the warhead is increased to 3.2 m. This is equivalent to a scenario where the missile is bended to a 60 degree "V"-shape. This way, the missile cannot turn into an orientation with a smaller cross-sectional area. The cross-section is approximately 6 m times 1.3 m, which is equivalent to the quoted diameter.

44. European Space Agency, *Launch Vehicle Catalogue* (Paris, F: European Space Agency, 1989).

45. In this case, the stress exceeds the elastic limit at temperatures close to 550 K, which are not reached for this absorption.

46. Robert K. Freeman, Fred A. Rigby and Nicholas Morley, "Temperature-dependent Reflectance of Plated Metals and Composite Materials under Laser Irradiation," in *29th Plasmadynamics and Lasers Conference: Albuquerque, NM, 15.-18. Juni,* AIAA-98-2482 (Washington, DC: American Institute of Aeronautics/Astronautics, 1998).

47. David R. Lide, ed., *CRC Handbook of Chemistry and Physics: A Ready-reference Book of Chemical and Physical Data,* 88th ed. 2007–2008 (Boca Raton, FL: CRC, 2007).

48. Dwight E. Gray, ed., *American Institute of Physics handbook,* 3. Auflage (New York: McGraw-Hill, 1972).

49. Lockheed Martin Missiles and Space, *Hubble Space Telescope Servicing Mission 3A—Media Reference Guide,* K9322, technical report (Washington, DC: NASA, 1999), http://hubble.nasa.gov/a_pdf/news/SM3A-MediaGuide.pdf (accessed Sept. 23, 2008).

50. Charles P. Vick, *Improved—Advanced Crystal/IKON/"KH-12" Reconnaissance Imaging Spacecraft* (2007), http://www.globalsecurity.org/space/systems/kh-12.htm (accessed Sep. 23, 2008).

51. U.S. Senate Committee On Armed Services, *Hearing to Receive Testimony in Review of the Defense Authorization Request for Fiscal Year 2010 and the Future Years Defense Program, 14 May 2009,* Transcript of Hearing (2009), p. 21, http://armed-services.senate.gov/Transcripts/2009/05%20May/09-31%20-%205-14-09.pdf (accessed May 19, 2009).

52. Jan Stupl, *Untersuchung der Wechselwirkung von Laserstrahlung mit Strukturelementen von Raumflugkörpern*. Project Summary, Project funded by the Berghof Foundation for Conflict Studies GmbH, Principal investigators: Prof. Dr. Martin B. Kalinowski (ZNF) und Prof. Dr. Götz Neuneck (IFSH) (Hamburg: Institute for Peace Research, Security Policy at the University of Hamburg (IFSH)/Carl Friedrich von Weizsäcker Center for Science and Peace Research (ZNF), march 2008).

53. Anthony E. Siegman, *LASERS* (Mill Valley, CA, USA: University Science Books, 1986).

54. Ibid., p. 676.

55. Mitchell H. Fields et al., "Initial results from the Advanced-Concepts Laboratory for Adaptive Optics and Tracking," in *Laser Weapons Technology,* vol. 4034, Proceedings of SPIE (Bellingham, WA: SPIE, 2000), 116–127.

56. Anthony E. Siegman, "Defining the Effective Radius of Curvature for a Nonideal Optical Beam," *IEEE Journal of Quantum Electronics* 27, no. 5 (May 1991): 1146–1148, ISSN: 0018-9197, doi:10.1109/3.83370; Anthony E. Siegman, G. Nemes and J. Serna, "How to (Maybe) Measure Laser Beam Quality," *in DPSS (Diode Pumped Solid State) Lasers: Applications and Issues* (Optical Society of America, 1998), MQ1.

57. Gail P. Anderson et al., "MODTRAN4: Radiative Transfer Modeling for Remote Sensing," in *Algorithms for Multispectral, Hyperspectral, and Ultraspectral Imagery VI,* vol. 4049, 1 (Orlando, FL, USA: SPIE, 2000), 176–183, doi: 10.1117/12.410338; Alexander Berk et al., *MODTRAN4 User's Manual,* technical report (Hanscom Air Force Base, MA, 1999); Alexander Berk, Lawrence S. Bernstein and David C Robertson, *MODTRAN: A Moderate Resolution Model for LOWTRAN 7,* GL-TR-89-0122, technical report (Hanscom Air Force Base, MA: Air Force Geophysics Laboratory, 1989), http://handle.dtic.mil/100.2/ADA214337 (accessed May 2, 2008).

58. Ernest Bauer and Robert R. Beland, *Atmospheric Effects on Airborne Lasers for Tactical Missile Defense: Clouds and Turbulence,* IDA D-1082; ADA277805, technical report (Alexandria, VA: Institute For Defense Analyses, Jan. 1, 1993), http://handle.dtic.mil/100.2/ADA277805 (accessed May 2, 2008).

59. Larry C. Andrews, *Field Guide to Atmospheric Optics,* SPIE field guides (Bellingham, WA: SPIE Press, 2004).

60. Lewis Fry Richardson, *Weather Prediction by Numerical Process* (Cambridge, UK: Cambridge University Press, 1922); Andrei Nikolaevich Kolmogorov, "The local structure of turbulence in incompressible viscous fluids for very large Reynolds number," (new release: Proc. Roy. Soc. Lond. A 434 (1991):9–13), *Dokl. Akad. Nauk SSSR* 30 (1941): 299–303.

61. Robert R. Beland, "Propagation through Atmospheric Optical Turbulence," in *Atmospheric Propagation of Radiation,* vol. 2, The infrared and electro-optical systems handbook (Ann Arbor, Mich.: Infrared Information Analysis Center/SPIE Optical Engineering Press, 1993), p. 168 ff.

62. For details explaining the validity of the equation see Barton et al., "Report of the American Physical Society Study Group on Boost-Phase Intercept Systems for National Missile Defense: Scientific and Technical Issues," p. 393.

63. *Ibid.*, p. 305.

64. Andrews, *Field Guide to Atmospheric Optics,* p. 11.

65. Steven Kuhta et al., *Theater Missile Defense: Significant Technical Challenges Face the Airborne Laser Program,* GAO/NSIAD-98-37, technical report, Report to the Ranking Minority Member, Committee on National Security, House of Representatives (United States General Accounting Office (GAO), Oct. 23, 1997).

66. Barton et al., "Report of the American Physical Society Study Group on Boost-Phase Intercept Systems for National Missile Defense: Scientific and Technical Issues," p. 391 ff.

67. Andrews, *Field Guide to Atmospheric Optics;* Robert K. Tyson and Benjamin W. Frazier, *Field Guide to Adaptive Optics,* SPIE Field Guides (Bellingham, WA: SPIE Press, 2004); Smith, *Atmospheric Propagation of radiation.*

68. Richard J. Sasiela, *Electromagnetic Wave Propagation in Turbulence. Evaluation and Application of Mellin Transforms,* Springer series on wave phenomena ; 18 (Berlin:

Springer, 1994); John W. Strohbehn, *Laser Beam Propagation in the Atmosphere,* Topics in applied physics; 25 (Berlin: Springer, 1978).

69. Sasiela, *Electromagnetic Wave Propagation in Turbulence. Evaluation and Application of Mellin Transforms,* p. 164.

70. Sometimes lasers are employed to create artificial guide stars in certain atmospheric layers around 20 km and 90 km, see Robert K. Tyson, *Principlpes of Adaptive Optics, 2* ed. (Chestnut Hill, MA: Academic Press Inc., 1997), p. 81. For the case of missile defense, these altitudes will not necessarily be useful to place a beacon, as the missile might be targeted at an altitude different from 20 km or 90 km.

71. Kenneth W. Billman et al., "ABL Beam Control Laboratory Demonstrator," *in Airborne Laser Advanced Technology II,* vol. 3706, 1 (Orlando, FL, USA: SPIE, 1999), S. 172–179, doi: 10.1117/12.356954; Charles Higgs et al., "Adaptive Optics Compensation using Active Illumination," *in Airborne Laser Advanced Technology,* vol. 3381, 1 (Orlando, FL, USA: SPIE, 1998), 47–56, doi:10.1117/12.323954.

72. Barton et al., "Report of the American Physical Society Study Group on Boost-Phase Intercept Systems for National Missile Defense: Scientific and Technical Issues," p. 323.

73. *Ibid.*, p. 391 ff.

74. Phillip D. Stroud, "Anisoplanatism in Adaptive Optics Compensation of a Focused Beam with use of Distributed Beacons," *Journal of the Optical Society of America* A 13, no. 4 (1996): 868–874.

75. Barton et al., "Report of the American Physical Society Study Group on Boost-Phase Intercept Systems for National Missile Defense: Scientific and Technical Issues," p. 298.

76. Shirley Enguehard, *private email communication with Shirley Enguehard, Sr. Research Physicist, AMP Research, Inc, 19–24 September 2008* (2008); Shirley Enguehard and Brian Hatfield, "Incoherency and Multiple Laser Guide Stars," in *NOAO Workshop on the Reduction of Gemini AO Data* (2001), AMP-01-05-1–AMP-01-05-21.

77. Barton et al., "Report of the American Physical Society Study Group on Boost-Phase Intercept Systems for National Missile Defense: Scientific and Technical Issues," p. 405.

78. Boeing, *Technical Characteristics—Boeing 747–400* (2007), http://www.boeing.com/commercial/747family/pf/pf_400_prod.html (accessed Apr. 16, 2009).

79. This is a result of the envisioned figure-"8" flight path of the ABL aircraft, see Barton et al., "Report of the American Physical Society Study Group on Boost-Phase Intercept Systems for National Missile Defense: Scientific and Technical Issues," p. 339. In addition to this geometric requirement, a perpendicular beam exit is favorable to avoid heating the air in the path of the beam. This heating would introduce further beam degradation, see *ibid.*, p. 408 ff.

80. Jack L. Button, "Comparison of Vertical Profile Turbulence Structure with Stellar Observations," *Appl. Opt.* 12, no. 8 (1973): 1785–1793.

81. In general, an optimization between time delay-anisoplanatism and angular anisoplanatism could minimize the effects of anisoplanatism, as Barton et al. have noted. For this case study, calculations show that improvements to pure delay anisoplanatism are only marginal.

82. Barton et al., "Report of the American Physical Society Study Group on Boost-Phase Intercept Systems for National Missile Defense: Scientific and Technical Issues," p. 323.

83. Missile Defense Agency, *Fact Sheet—The Airborne Laser,* document number 09-FS-0004 (2009), http://www.mda.mil/mdalink/pdf/laser.pdf (accessed July 8, 2009).

84. Michael J. Gething, ed., *Jane's Electro-Optic Systems 2003–2004,* Jane's electro-optic Systems (Coulsdon: Jane's Information Group, 2003), p. 491.

85. Barton et al., "Report of the American Physical Society Study Group on Boost-Phase Intercept Systems for National Missile Defense: Scientific and Technical Issues," p. 314.

86. *Ibid.*, p. 314.

87. United Nations Monitoring, Verification and Inspection Commission, *Compendium of Iraq's Proscribed Weapons Programmes in the Chemical, Biological and Missile areas* (United Nations, 2007), p. 578, http://www.un.org/depts/unmovic/new/pages/compendium.asp (accessed July 6, 2008).

88. L. I. Balabukh et al., *The Bases of the Structural Mechanics of Rockets,* English translation of L. I. Balabukh et al., *Osnovy Stroitel not Mekhaniki Raket* (Moskau: Vyssh. Shkola, 1969). (Wright-Patterson Air Force Base, OH and Springfield, VA: United States Air Force Systems Command—Foreign Technology Division/United States National Technical Information Service NTIC, 1970), p. 585.

89. David Holloway et al., *Iran's Nuclear and Missile Potential—A Joint Threat Assessment by U.S. and Russian Technical Experts* (EastWest Institute, New York, NY, 2009), http://docs.ewi.info/JTA. pdf (accessed June 3, 2009); Robert H. Schmucker, "3rd World Missile Development—A New Assessment Based on UNSCOM Field Experience and Data Evaluation," in *12th Multinational Conference on Theater Missile Defense: Responding to an Escalating Threat, June 1–4, 1999, Edinburgh, Scotland* (1999).

90. R. W. Lewis et al., *The Finite Element Method in Heat Transfer Analysis* (Chichester, UK: Wiley, 1996).

91. Stupl, *Untersuchung der Wechselwirkung von Laserstrahlung mit Strukturelementen von Raumflugkörpern*, chapter 3.4.

92. *Ibid.*

93. United Nations Monitoring, Verification and Inspection Commission, *Compendium of Iraq's Proscribed Weapons Programmes in the Chemical, Biological and Missile Areas,* for example p. 577.

94. United Nations Monitoring, Verification and Inspection Commission, *Compendium of Iraq's Proscribed Weapons Programmes in the Chemical, Biological and Missile Areas',* Forden, "Ballistic Missile Defense: The Airborne Laser."

95. Wright and Kadyshev, "An Analysis of the North Korean Nodong Missile".

96. Freeman, Rigby, and Morley, "Temperature-dependent Reflectance of Plated Metals and Composite Materials under Laser Irradiation."

97. Lide, *CRC Handbook of Chemistry and Physics: A Ready-reference Book of Chemical and Physical Data.*

98. Freeman, Rigby, and Morley, "Temperature-dependent Reflectance of Plated Metals and Composite Materials under Laser Irradiation."

99. Merrill Cohen and John P. Doner, *Infrared Reflectance Spectra for Selected Paint Pigments,* AD0729354, technical report, CCL Report No. 293 (Aberdeen Proving Ground, MD: U. S. Army, Aberdeen Research & Development Center, Coating & Chemical Laboratory, July 1971), http://handle.dtic.mil/100.2/AD729354 (accessed June 3, 2008); D. K. Edwards and W. M. Hall, *Far-Infrared Reflectance of Spacecraft Coatings,* 32-873, technical report (Pasadena, CA: Jet Propulsion Laboratory, California Institute

of Technology/NASA, Jan. 31, 1966), http://hdl.handle.net/2060/19660010344 (accessed June 3, 2008).

100. Ernst U. Schlünder, "Physical properties," in *Heat Exchanger Design Handbook,* vol. 5 (New York, NY: Hemisphere Publishing/Taylor & Francis, 1989), chapter 5.5.7, David G. Gilmore, *Spacecraft Thermal Control Handbook, Volume 1—Fundamental Technologies* (Reston, VA: American Institute of Aeronautics & Astronautics, 2002), p. 795–797.

101. Balabukh et al., *The Bases of the Structural Mechanics of Rockets,* p. 428 ff.

102. Kevin L. Zondervan and Derek W. Beck, "Approximate Closed-Form Expression for the Probability of Burst of a Pressurized Metal Cylinder Irradiated by a High-Energy Laser," in *33rd Plasmadynamics and Lasers Conference, 20–23 May, 2002, Maui, HI,* AIAA-2002-2220 (Reston, VA: American Insitute of Aeronautics/ Astronautics, 2002); Herbert Oertel, *Aerothermodynamik* (Berlin: Springer, 1994).

103. Zondervan and Beck, "Approximate Closed-Form Expression for the Probability of Burst of a Pressurized Metal Cylinder Irradiated by a High-Energy Laser".

104. European Space Agency, *Launch Vehicle Catalogue.*

105. Sigmund, *Metal.yield.svg,* public domain (2007), http://commons.wikimedia.org/wiki/File:MetaL_yield.svg (accessed June 3, 2009).

106. John Gilbert Kaufman, ed., *Properties of Aluminum Alloys: Tensile, Creep, and Fatigue Data at High and Low Temperatures* (Materials Park, OH: ASM International, 1999).

107. Balabukh et al., *The Bases of the Structural Mechanics of Rockets,* p. 463.

108. Stupl, *Untersuchung der Wechselwirkung von Laserstrahlung mit Strukturelementen von Raumflugkörpern*, chapter 4.3.

109. The cylinders are manufactured by Ball Packaging Europe GmbH and are usually used to store a variety of alcoholic beverages.

110. T. Bothe et al., "Erzeugung und Auswertung von Objektangepassten Inversen Projektions-mustern," *Technisches Messen* 70, no. 2 (2003): 99–103; Wansong Li et al., "Applications of Inverse pattern projection," in *Optical Measurement Systems for Industrial Inspection III,* vol. 5144, Proceedings of SPIE (Bellingham, WA: SPIE, 2003), 493–503; Wansong Li et al., "Object Adapted Pattern Projection-Part I: Generation of Inverse Patterns," *Optics and Lasers in Engineering* 41, no. 1 (Jan. 2004): 31–50.

111. United Nations Monitoring, Verification and Inspection Commission, *Compendium of Iraq's Proscribed Weapons Programmes in the Chemical, Biological and Missile areas.*

112. Wright and Kadyshev, "An Analysis of the North Korean Nodong Missile".

113. Forden, "Ballistic Missile Defense: The Airborne Laser".

114. Wright and Kadyshev, "An Analysis of the North Korean Nodong Missile".

115. Forden, "GUI Missile Flyout: A General Program for Simulating Ballistic Missiles".

116. Beland, "Propagation through Atmospheric Optical Turbulence," p. 220.

117. COMSOL AB, *COMSOL Material Library,* Database, Version 3.4 (Stockholm, SE, 2007).

118. *Ibid.*

119. *Ibid.*

120. Schlünder, "Physical properties".

121. COMSOL AB, *COMSOL Material Library.*

122. *Ibid.*

123. *Ibid.*

124. Kaufman, *Properties of Aluminum Alloys: Tensile, Creep, and Fatigue Data at High and Low Temperatures.*